Supplementary Information

A Stable Open-Shell *Peri*-hexacene with Remarkable Diradical Character

Jinji Zhang,[1,†] Xiaojing Fang,[1,†] Weiwei Niu,[2,†] Yiming Yu,[1] Yanlin Hu,[1] Jiawen Sun,[1] Ying Xu,[1] Zhihua Zhou,[3] Heyuan Liu,[4] Xiaonan Fan,[4] Baishu Zheng,[3] Qing Jiang,[5*] Guangwu Li,[2,6*] Wangdong Zeng[1*]*

[1]School of Materials Science and Engineering, Hunan University of Science and Technology, Xiangtan 411201, China.

[2]Center of Single-Molecule Sciences, Institute of Modern Optics, Tianjin Key Laboratory of Micro-Scale Optical Information Science and Technology, College of Electronic Information and Optical Engineering, Nankai University, 38 Tongyan Road, Jinnan District, Tianjin 300350, China.

[3]Key Laboratory of Theoretical Organic Chemistry and Function Molecule of Ministry of Education, Hunan Provincial Key Laboratory of Controllable Preparation and Functional Application of Fine Polymers, School of Chemistry and Chemical Engineering, Hunan University of Science and Technology, Xiangtan 411201, China.

[4]School of Materials Science and Engineering, China University of Petroleum (East China), Qingdao, Shandong, 266580, China

[5]College of Chemistry and Bioengineering, Hunan University of Science and Engineering, Yongzhou, 425100, China.

[6]Shenzhen Research Institute of Nankai University, 16th Floor, Yantian Science & Technology Building, Haishan Street, Yantian District, Shenzhen, 518083, P. R. China.

[†]These authors contributed equally: Jinji Zhang, Xiaojing Fang, Weiwei Niu.

*e-mail: wangdong.zeng@hnust.edu.cn; zbaishu@163.com; qjiang198@163.com; ligw@nankai.edu.cn

Table of Contents

1. Supplementary Methods

1.1 General

Solvents were purified and dried by standard methods prior to use. Starting materials were obtained from commercial suppliers and used without further purification. Anhydrous methylbenzene and tetrahydrofuran (THF) were distilled under a nitrogen atmosphere over sodium hydride, respectively. Compound 3,10-dibromo-1,1-bis(3,5-di-tert-butylphenyl)-1H-cyclopenta[ghi]perylene[1] and 2,2'-((2,5-dibromo-1,4-phenylene)bis(ethyne-2,1-diyl))bis(1,3-dichlorobenzene)[2] were prepared according to the literatures. Column chromatography was performed on silica gel（200-300 mesh) and reactions were monitored by thin layer chromatography (TLC) using silica gel GF254 plates to visualize the course of reaction.

All the ^{1}H NMR spectra were recorded on a 400 MHz spectrometer and ^{13}C NMR data were collected on a 125 MHz spectrometer. All chemical shifts are quoted in ppm, relative to tetramethylsilane, using the residual solvent peak as a reference standard. The following abbreviations were used to explain the multiplicities: s = singlet, d = doublet, m = multiplet. Matrix-Assisted Laser Desorption / Ionization Time of Flight Mass Spectrometry (MALDI-TOF MS) were performed on a Finnigan MAT TSQ 7000 instrument. UV-vis-NIR absorption spectra was recorded on a Shimadzu UV-3600 spectrophotometer. Cyclic voltammetry (CV) and differential pulse voltammetry (DPV) were performed in dry DCM on a Chenhua 650D electrochemical using a three-electrode cell with a glassy carbon working electrode, a platinum wire counter electrode, and a Ag/AgCl reference electrode in anhydrous solvents containing tetra-n-butyl-ammoniumhexa-fluorophosphate (TBAPF$_6$, 0.1 M) as supporting electrolyte at 298 K. The potential was externally calibrated against the ferrocene/ferrocenium couple. Electron paramagnetic resonance (ESR) spectra were obtained with a JES-FA200 spectrometer in a dry DCM. Transient absorption (TA) spectra were recorded using a femtosecond pump-probe detection system. The laser source was an ultrafast laser amplifier (Coherent) with a central wavelength of 800 nm, a repetition rate of 1 kHz, a pulse width of 100 fs, and a pulse energy of 6 mJ. The output laser beam was divided into two paths using a beam splitter. The reflected beam was directed into a pump optical parametric amplifier (OPA, Spectra-Physics, TOPAS) to generate pump beams with tunable wavelengths ranging from 250 to 2500 nm. A chopper reduced the pump beam's frequency to 500 Hz for sample excitation, and its intensity was adjusted using a continuously variable neutral density filter wheel. The transmitted beam was used to generate a continuous white light (350–800 nm) via a CaF$_2$ crystal, serving as the probe beam. After passing through the sample, the probe beam was collected by a fiber-coupled spectrometer. An optical delay line controlled the delay between the pump and probe beams. For the fs-TA experiment, the excitation wavelength was set at 610 nm. The sample concentration was 0.1 mM, and the solvent used was DCM.

EPR test. CW-EPR spectra were recorded using a Bruker Elexsys E580 spectrometer equipped with a Superhigh sensitivity probehead (ω = 9.8 GHz). Pulsed EPR measurements were conducted on a SuperQ-FT spectrometer (ω = 33.7 GHz). The zero field splitting parameters were determined by fitting with the EasySpin package in Matlab. The pulsed-EPR experiment signals were acquired through the integration of the Hahn echo sequence ($\pi/2-\tau-\pi-\tau-$echo) with τ set to 400 ns. The T_1 value was assessed using the inversion recovery method ($\pi-\tau-\pi/2-\tau-\pi-\tau-$echo) and a four-step phase cycling protocol. The Tm value was derived by incrementing the τ value in the Hahn echo sequence with a 16-step phase cycling method. The durations of the $\pi/2$ and π pulses for T_1 and T_m measurements were 12 and 24 ns, respectively. Furthermore, the linearity of the oscillation frequency response to the B_1 field across various fields was quantified, verifying the detectability of Rabi cycles. The Rabi frequency (Ω) for the transition Ms→(Ms+1) of spin S adheres to the established formula:

$$\Omega_R^{M_s \leftrightarrow M_s+1} = g\mu_R B_1 \sqrt{S(S+1) - M_s(M_s+1)}, (Ms = -S,\ldots\ldots,S-1) \tag{1}$$

where g is the g-factor, μ_R is the Bohr magneton, and B1 is the magnetic field amplitude of the microwave pulse. During this study, the value of $g\mu_R B_1$ was standardized against a stable tris(2,4,6-trichlorophenyl)methyl radical (TTM, S = 1/2). The Rabi frequency is expected to show a linear relationship with the B_1 field, and assuming constant g values, the slope for an S = 1 species would be $\sqrt{2}$ times greater than that for an S = 1/2 species.

CW-EPR measurements were conducted on the sample in both solid and liquid states, with toluene serving as the solvent at a concentration of 80 μmol/mol in the liquid state, and temperature dependence was assessed. For pulsed EPR, the sample was measured in its liquid state, again with toluene as the solvent, but at a higher concentration of 160 μmol/mol, without performing temperature dependence tests.

A Quantum Design 7 Tesla SQUID-VSM system was available for the magnetic measurement of **1** in this work. Microcrystalline powder sample with a weight of 4-8 mg was sealed in a plastic capsule. Magnetic moment was measured in the temperature range of 2 to 300 K. The empty plastic capsule exhibited diamagnetic and its magnetic moment was measured for correction. After correction of diamagnetic contributions from the sample, sample holder and paramagnetic contamination, the magnetic data were fitted with Bleaney-Bowers equation:

$$\chi_M T = \frac{2N\beta^2 g^2}{k_B[3 + exp\left(-\frac{2J}{k_B T}\right)]} \tag{2}$$

where, -2J is correlated to the excitation energy from the singlet ground state to the triplet excited state.

## 1.2 Synthesis section

Synthesis of perylene-1-carbaldehyde
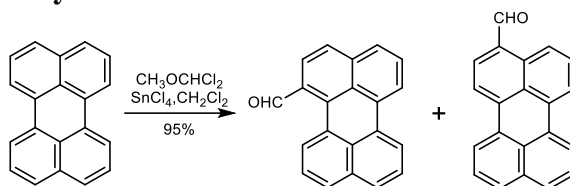
A suspension of perylene (6 g, 23.84 mmol) in CH_2Cl_2 (140 mL) was cooled to 0 °C in an ice bath under an argon atmosphere. $SnCl_4$ (5.76 mL, 49.2 mmol) was added in one portion, and then Cl_2CHOCH_3 (2.7 mL, 24.6 mmol) was added dropwise over 1 h, and the reaction was stirred for an additional 1 h with the solution temperature of 0 °C. The resulting suspension was warmed slowly to room temperature and then refluxed for 16 h. After cooling, water (200 mL) was added to quench the reaction and the organic layer was separated and washed by water, dried over Na_2SO_4. The crude mixture was subjected to silica gel column chromatography (hexane/DCM = 1:1) to afford the perylene-1-carbaldehyde and perylene-3-carbaldehyde as yellow solid (6.33 g, 95% yield). The conversion is nearly quantitative and based on ^{1}H NMR analysis; a mixture of 3-formylperylene perylene-1-carbaldehyde and 1-formylperylene perylene-3-carbaldehyde in the ratio of about perylene-1-carbaldehyde : perylene-3-carbaldehyde = 1:4 was obtained. Pure perylene-3-carbaldehyde can be separated by column chromatography, but no pure perylene-1-carbaldehyde could be obtained.

Synthesis of methyl perylene-1-carboxylate
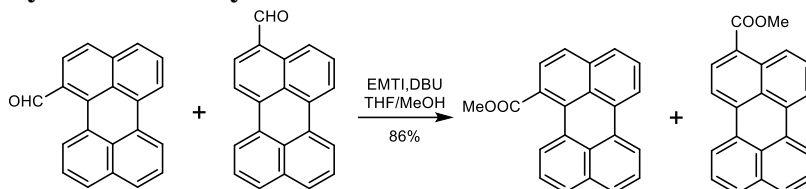
To a solution of 4-ethyl-1-methyl-4H- [1, 2, 4] triazol-1-ium iodide (EMTI, 650 mg, 2.7 mmol) in dry tetrahydrofuran (THF, 150 mL) and dry MeOH (150 mL), 1,8-diazabicyclo[5.4.0]undec-7-ene (DBU) (3.04 mL, 19.6 mmol) was added, a mixture of perylene-1-carbaldehyde and perylene-3-carbaldehyde (ca. 1:1, 5 g, 17.9 mmol) was then added, and the solution was stirred at 45 °C for 5 h. The solvent was then removed under vacuum. Brine was added and the reaction mixture was extracted with DCM, and the residue was subjected to flash column chromatography (hexane/DCM = 1:1) to yield the ester product methyl perylene-1-carboxylate and methyl perylene-3-carboxylate (4.75 g, 86 %). ^{1}H NMR ($CDCl_3$, 400 MHz): δ ppm 8.24 (d, 2H), 7.78-7.72 (m, 4H), 7.68 (d, 2H), 7.60-7.53 (m, 3H), 7.48 (t, 1H), 3.87 (s, 3H).

### Synthesis of 1,1-bis(3,5-di-tert-butylphenyl)-1H-cyclopenta[ghi]perylene
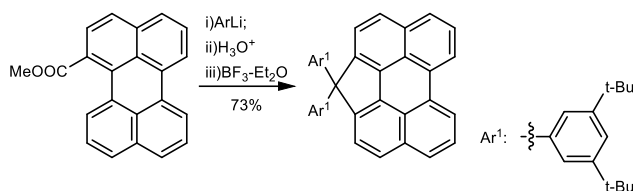
A solution of 3.5-di-tert-butyl-bromobenzene (1.8 g, 6.6 mmol) in dry THF (125 mL) was cooled to -78 °C under nitrogen atmosphere and n-BuLi (2.0 M in cyclohexane, 3.3 mL, 6.6 mmol) was added dropwise. The solution was stirred at -78 °C for 1 h. Then a solution of perylene-1 carboxylate in THF (480 mg, 1.5 mmol) was added dropwise. The mixture was slowly warmed up to room temperature and was stirred overnight. 50 mL of saturated aqueous $NaHCO_3$ was added to quench the reaction and the mixture was extracted with DCM. The combined organic layer was dried over sodium sulfate. The solvent was removed under reduced pressure and a brown liquid was obtained. Boron trifluoride diethyl etherate (2.5 mL) was added to a solution of the as-prepared brown liquid in DCM (150 mL) at room temperature under nitrogen atmosphere and the solution turned dark immediately. After stirring for 5 h, methanol (25 mL) and water (50 mL) were added to quench the reaction. Brine was added and the reaction mixture was extracted with DCM. The organic layer was dried over sodium sulfate and then evaporated to dryness. The crude mixture was subjected to silica gel column chromatography (hexane/DCM = 10/1) to afford the1,1-bis(3,5-di-tert-butylphenyl)-1H-cyclopenta[ghi]perylene (0.68 g, 73% yield for two steps from perylene-1-carboxylate). ^{1}H NMR (CDCl3, 400 MHz): δ ppm 8.13 (d, 2H), 7.75 (d, 2H), 7.60 (d, 2H), 7.56 (m, 4H), 7.24 (s, 2H), 7.14 (s, 4H), 1.19 (s, 36H)

Synthesis of 3,10-dibromo-1,1-bis(3,5-di-tert-butylphenyl)-1H-cyclopenta[ghi]perylene
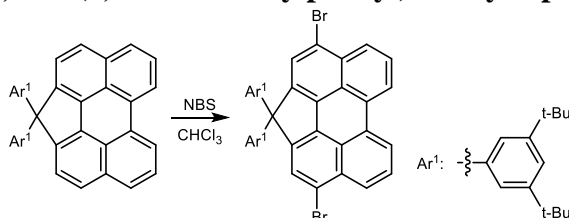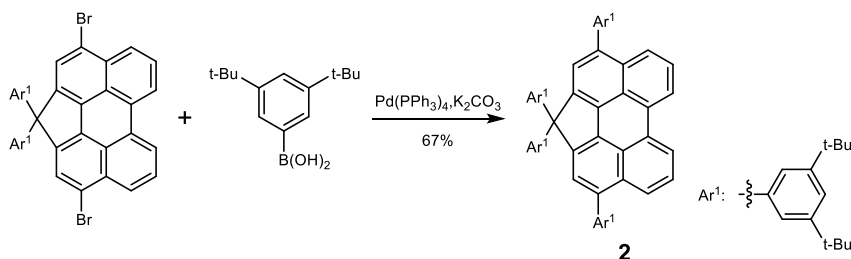

A solution of 1,1-bis(3,5-di-tert-butylphenyl)-1H-cyclopenta[ghi]perylene (320 mg, 0.5 mmol) in CHCl3 (50 mL) was added N bromosuccinimide (NBS) (180 mg, 1.1 mmol), and the mixture was stirred at 0 °C for 30 min. Brine was added and the reaction mixture was extracted with DCM. The organic layer was dried over sodium sulfate and then evaporated to dryness. The crude mixture was subjected to silica gel column chromatography (hexane/DCM = 5/1) to afford the 3,10-dibromo-1,1-bis(3,5-di-tert-butylphenyl)-1H-cyclopenta[ghi]perylene as yellow solid (425 mg, 90% yield). ^{1}H NMR (CDCl3, 400 MHz): δ ppm 8.18 (d, 2H), 7.88 (s, 2H), 7.83 (s, 2H), 7.76 (t, 2H),7.28 (d, 2H), 7.04 (s, 4H), 1.24 (d, 36H).

Synthesis of Compound 5

5
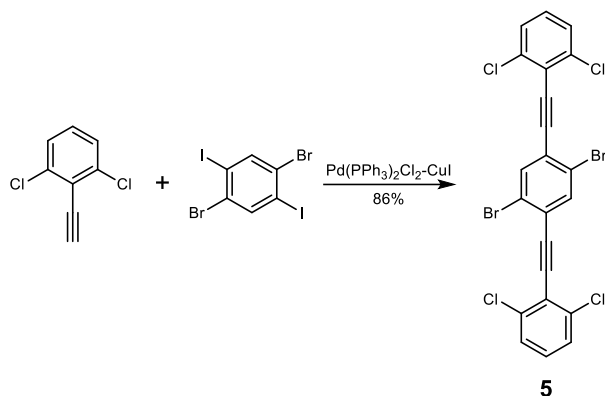
A mixture of compound 1,3-dichloro-2-ethynylbenzene (2.00 g, 11.7 mmol), 1,4-dibromo-2,5-diiodobenzene (2.67 g, 5.48 mmol), triethylamine (20 mL), toluene (50 mL), CuI (0.20 g, 1.05 mmol) and Pd(PPh$_3$)Cl$_2$ (0.73 g, 1.05 mmol) was carefully degassed by three freeze-pump-thaw cycles, and then was stirred at room temperature for 5 hours under argon atmosphere. A gray solid precipitated out during the reaction, and after filtration and washing several times by cold toluene (5×40 mL), compound **5** was obtained as a gray solid (2.69 g, yield 86%), which was directly used for next step without further purification. Due to its poor solubility (even 0.1 mg sample could not be dissolved in 2 mL toluene with sonication and heating), the ^{1}H NMR spectra of compound **5** cannot be recorded in commonly used solvents such as CDCl$_3$, d$_8$-THF, d$_6$-benzene and d$_8$-toluene.

Synthesis of Compound 2

2

A 500ml two-necked round bottom flask was charged with 3,10-dibromo-1,1-bis(3,5-di-tert-butylphenyl)-1H-cyclopenta[ghi]perylene[1] (1.00 g, 1.25 mmol), (3,5-di-tert-butylphenyl)boronic acid (871 mg, 3.72 mmol), 1M aq. K$_2$CO$_3$ (7.0 mL), ethanol (10.0 mL), toluene (50.0 mL) and purged with argon for 30 min. Pd(PPh$_3$)$_4$ (145 mg, 10 mol%) was added under argon. The resultant mixture was then heated at 100 °C overnight. After cooling to room temperature, brine was added and the reaction mixture was extracted with DCM. The organic layer was dried over sodium sulfate and then evaporated to dryness. The crude mixture was subjected to silica gel column chromatography (hexane) to afford the title product **2** as yellow solid (851 mg, 67% yield). ^{1}H NMR (CDCl$_3$, 400 MHz): δ ppm 8.20 (d, 2H), 7.84 (d, 2H), 7.62 (s, 2H), 7.54 (t, 2H), 7.46 (s, 2H), 7.41 (s, 4H), 7.26 (d, 6H), 1.39 (s, 36H), 1.20 (s, 36H); ^{13}C NMR (CDCl$_3$, 125 MHz): δ ppm 150.63, 150.14, 142.04, 135.10, 133.03, 127.40, 126.32, 124.62, 122.85,

120.93, 120.51, 35.07, 34.98, 31.70, 31.63, 29.82; HRMS (MALDI-TOF, m/z): calcd for $C_{77}H_{92}$ [M+H]$^+$, 1016.7199; found 1016.7210 (error = +1.1 ppm).

Synthesis of Compound 3
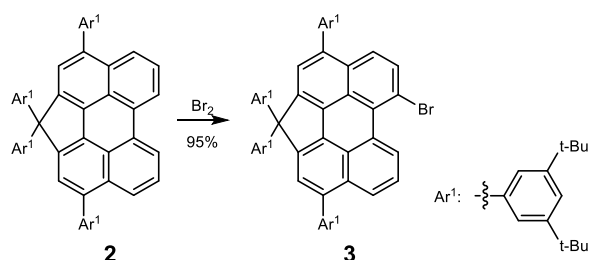
To the solution of compounds 2 (1.00 g, 0.98 mmol) in dry CH_2Cl_2 (100 mL) was added bromine (1.2 mmol) in DCM, and the mixture was stirred at 0 °C for 30 min, then poured into aqueous $Na_2S_2O_3$ (20 mL) and the combined organic layers were washed with brine and dried over anhydrous sodium sulfate. The crude mixture was subjected to silica gel column chromatography (hexane) to afford the title product 3 as yellow solid (1.02 g, 95% yield). ^{1}H NMR (CDCl$_3$, 400 MHz): δ 9.64 (d, 1H), 7.93 (d, 1H), 7.74 (d, 2H), 7.64-7.57 (m, 4H), 7.47 (d, 2H), 7.40 (d, 2H), 7.36 (d, 2H), 7.24 (s, 2H), 7.20 (d, 4H), 1.38 (s, 36H), 1.19 (s, 36H); ^{13}C NMR (CDCl$_3$, 125 MHz): δ 150.79, 150.68, 150.22, 147.05, 146.09, 141.94, 140.66, 140.36, 140.18, 139.61, 135.38, 134.35, 134.16, 132.37, 132.00, 131.11, 130.90, 128.65, 126.87, 126.17, 126.05, 125.84, 124.70, 124.62, 122.86, 121.12, 121.03, 120.61, 118.98, 70.94, 35.08, 34.99, 31.71, 31.62, 29.82, 27.03; HRMS (MALDI-TOF, m/z): calcd for $C_{77}H_{91}Br$[M+H]$^+$, 1094.6304; found 1094.6312 (error = +0.73 ppm).

Synthesis of Compound 4
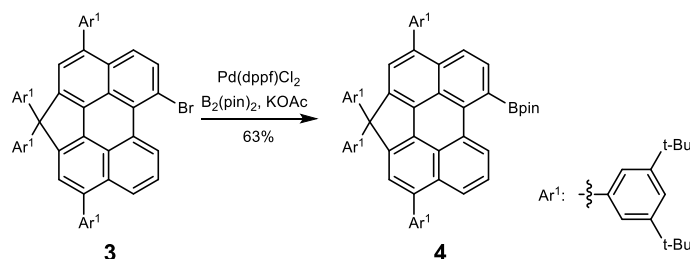
A mixture of **3** (1.5 g, 1.37 mmol), bis (pinacolato) diboron (522 mg, 2.05 mmol), [1,1'-bis (diphenylphosphino) ferrocene]palladium (II) dichloride dichloromethane adduct (112 mg, 10 mol%) and potassium acetate (402 mg, 4.10 mmol) in a solution of dioxane (50 mL) was stirred and heated at 80 °C under nitrogen atmosphere for 12 h. After cooling, the solvent was removed under reduced pressure. The crude mixture was subjected to silica gel column chromatography (hexane/DCM = 3:1) to afford the title product **4** as yellow solid (0.86 g, 63% yield). ^{1}H NMR (CDCl$_3$, 400 MHz): δ 8.27 (d, 1H), 7.86 (t, 2H), 7.64-7.60 (m, 3H), 7.49-7.45 (t, 3H), 7.41 (d, 4H), 7.23 (t, 6H), 1.52 (s, 12H), 1.38 (s, 36H), 1.19 (s, 36H); ^{13}C NMR (CDCl$_3$, 125 MHz): δ 150.55, 150.52, 150.07, 146.38, 146.20, 141.99, 140.70, 140.66, 139.59,

139.28, 138.07, 135.19, 134.90, 133.73, 132.67, 132.02, 131.97, 84.28, 74.41, 35.01, 34.92, 24.92; HRMS (MALDI-TOF, m/z): calcd for $C_{83}H_{103}BO_2[M+H]^+$, 1142.8051; found 1142.8060 (error = +0.79 ppm).

Synthesis of Compound 6
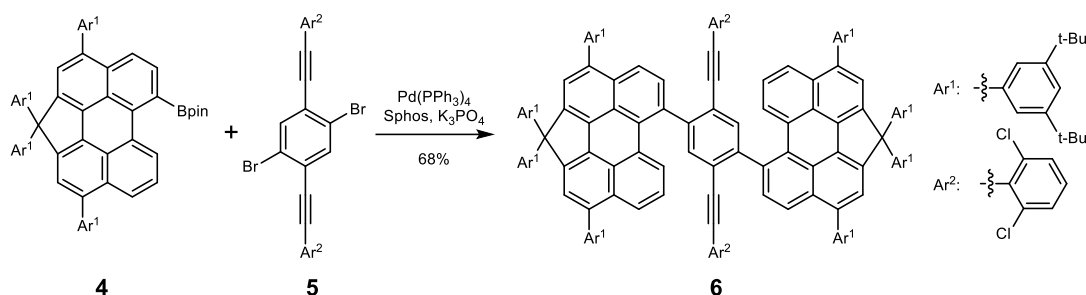
A mixture of **4** (571 mg, 0.50 mmol), **5**[2] (95 mg, 0.17 mmol), 1M aq. K_3PO_4 (2 mL) and toluene (30 mL) was purged with nitrogen for 30 min. $Pd(PPh_3)_4$ (20 mg, 10 mol%) and 2-Dicyclohexylphosphino-2',6'-dimethoxybiphenyl (14 mg, 20 mol%) was added under nitrogen. The mixture was stirred and heated at 85 °C under nitrogen atmosphere for overnight. After cooling to room temperature, water was added and the reaction mixture was extracted with DCM. The organic layer was dried over sodium sulfate. The crude mixture was subjected to silica gel column chromatography (hexane/DCM = 15:1) to afford the pure product **6** as yellow solid (276 mg, 68% yield). ^1H NMR (CDCl$_3$, 400 MHz): δ 8.05 (m, 2H), 7.99-7.90 (m, 3H), 7.80 (d, 1H), 7.75 (d, 1H), 7.65 (m, 4H), 7.54 (d, 1H), 7.47 (d, 7H), 7.43 (m, 4H), 7.39 (d, 5H), 7.33 (d, 4H), 7.27 (s, 2H), 7.24 (d, 6H), 6.99 (d, 4H), 6.94 (m, 2H), 1.40 (d, 36H), 1.34 (s, 36H), 1.23 (s, 36H), 1.20 (s, 36H); ^{13}C NMR (CDCl$_3$, 125 MHz): δ 149.47, 149.40, 148.99, 148.90, 148.87, 145.59, 145.54, 145,47, 145.43, 145.11, 145.03, 141.34, 141.30, 140.90, 140.84, 139.65, 138.74, 138.67, 138.40, 138.24, 136.81, 136.21, 136.16, 134.60, 134.55, 134.10, 133.83, 133.20, 133.10, 132.45, 132.22, 131.01, 130.94, 130.84, 130.79, 130.60, 130.49, 129.32, 129.20, 127.99, 127.82, 126.28, 126.16, 126.08, 125.98, 124.98, 124.72, 124.61, 124.25, 123.55, 123.51, 123.34, 121.98, 121.95, 121.88, 121.74, 119.75, 119.67, 119.35, 119.26, 113.05, 97.10, 97.05, 87.89, 69.93, 33.93, 33.88, 33.84, 30.89, 30.52, 28.67, 28.48, 28.33, 28.13, 27.91, 25.87, 21.66, 20.43, 13.10; HRMS (MALDI-TOF, m/z): calcd for $C_{176}H_{190}Cl_4$ $[M+H]^+$, 2443.3622; found 2443.3645 (error = +0.94 ppm).

Synthesis of Compound 7

9
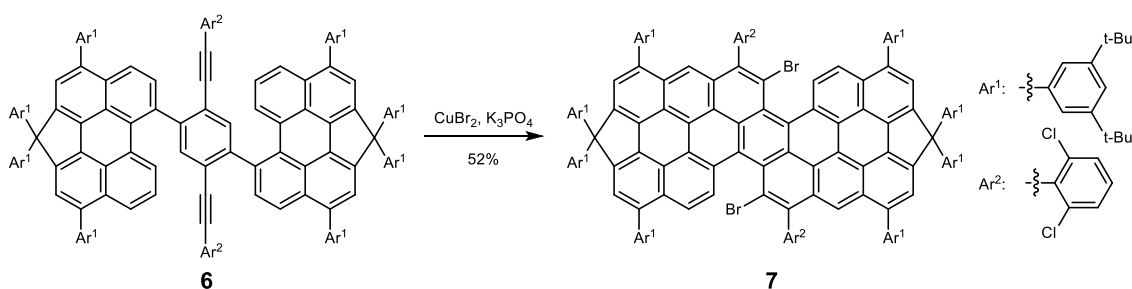
In a nitrogen-filled glove box, a mixture of **6** (800 mg, 0.33 mmol), CuBr$_2$ (875 mg, 3.92 mmol), K$_3$PO$_4$ (70 mg, 0.033 mmol) and anhydrous DCE (20 mL) were sequentially added to a 100 mL solution storage bottles equipped with a stir bar. The reaction mixture was heated at 85 °C for 72 h under nitrogen. After cooling to room temperature, water was added and the reaction mixture was extracted with DCM. The organic layer was dried over sodium sulfate. The crude mixture was subjected to silica gel column chromatography (hexane/DCM = 10:1) to afford the pure product **7** as green solid (450 mg, 52% yield). ^{1}H NMR (CDCl$_3$, 400 MHz): δ 9.21 (d, 2H), 8.59 (s, 2H), 8.45 (d, 2H), 8.23 (d, 4H), 7.70-7.67 (m, 6H), 7.64 (d, 4H), 7.57 (m, 6H), 7.47-7.40 (m, 6H), 7.34 (t, 2H), 7.17 (t, 2H), 7.08 (d, 4H), 1.45 (s, 36H), 1.40 (s, 36H), 1.28 (s, 36H), 1.09 (s, 36H); ^{13}C NMR (CDCl$_3$, 125 MHz): δ 150.82, 150.41, 150.19, 130.23, 128.89, 128.52, 124.74, 123.21, 122.70, 120.87, 120.61, 35.20, 35.11, 35.03, 34.89, 31.73, 31.52, 29.81, 22.81, 14.26; HRMS (MALDI-TOF, m/z): calcd for C$_{176}$H$_{184}$Br$_2$Cl$_4$[M+H]$^+$, 2595.1519; found 2595.1545 (error = +1.0 ppm).

Synthesis of Compound 8
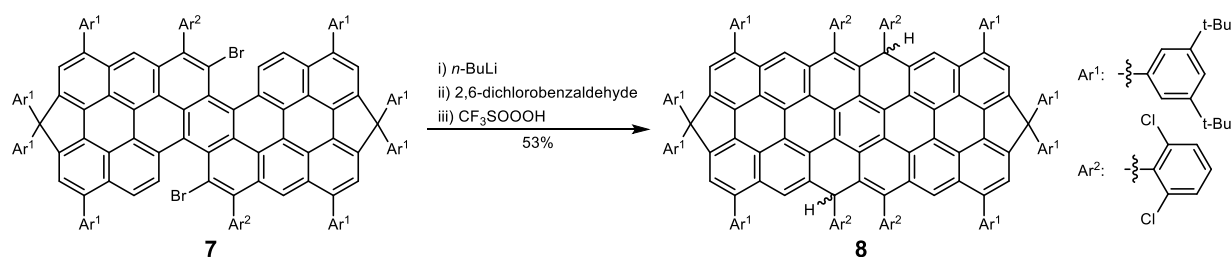
Compound **7** (300 mg, 0.12 mmol) was dissolved in anhydrous toluene (20 mL). The solution was cooled to -15 °C and 1.6 M n-BuLi (0.22 mL, 0.35 mmol) in hexane was added slowly. After stirring for 30 min, 2,6-Dichlorobenzaldehyde (101 mg, 0.58 mmol) in toluene was injected dropwise. The solution was stirred at room temperature for 2 h and then the reaction was quenched with MeOH. The reaction mixture was mixed with EtOAc (30 mL) and the organic phase was washed with water. After drying over Na$_2$SO$_4$, the organic solvent was evaporated under reduced pressure to afford viscous green oil. This was redissolved in anhydrous DCM (20 mL) and mixed with CF$_3$SOOOH (0.40 mL, 4.52 mmol). After 30 min stirring, the reaction was quenched with triethylamine. The solution was diluted with DCM and washed by brine. The organic layer was separated, dried over Na$_2$SO$_4$ and evaporated in vacuo. The crude mixture was subjected to silica gel column chromatography (hexane/DCM = 10:1) to afford the configurational isomers of product **8** as green solid (168 mg, 53% yield). ^{1}H NMR (CDCl$_3$, 400 MHz): δ 8.45 (s, 2H), 8.13 (d, 4H), 7.78 (s, 2H), 7.51-7.28 (m, 26H), 7.22 (t, 4H), 7.12-7.07 (m, 4H), 6.96-6.90 (m, 4H), 1.40 (m, 72H), 1.17 (d, 72H); HRMS (MALDI-TOF, m/z): calcd for C$_{190}$H$_{190}$Cl$_8$ [M+H]$^+$, 2751.2376; found 2751.2412 (error = +1.3 ppm).

Synthesis of Compound 1
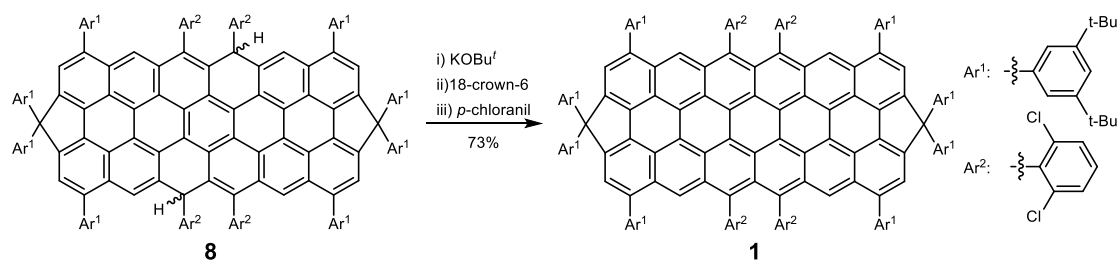
In a nitrogen-filled glove box, under argon atmosphere and in the dark, a 20 ml vial containing a magnetic stir bar was charged with **8** (50 mg, 0.018 mmol), tert-butoxide potassium (20.4 mg, 0.182 mmol), 18-crown-6 (48.0 mg, 0.182 mmol) and THF (10 mL). The resulting mixture was stirred at room temperature for 6 h, then p-chloranil (11.6 mg, 0.047 mmol) was added. The mixture was kept stirred for 20 min and then the solvent was removed under reduced pressure at room temperature. The resulting residue was directly subjected to flash chromatography (silica gel was neutralized with Et_3N, Hexane/DCM = 3:1). The cyan solid of pure product **1** was obtained (36.5 mg, 73% yield). HRMS (MALDI-TOF, m/z): calcd for $C_{190}H_{188}Cl_8[M+H]^+$, 2479.2219; found 2479.2274 (error = +2.0 ppm).

1.3 Density functional theory (DFT) calculations

Theoretical calculations were performed with the Gaussian16 program suite.[3] All calculations were carried out using the density functional theory (DFT) method with unrestricted Becke's three-parameter hybrid exchange functionals and the Lee-Yang-Parr correlation functional (UB3LYP) employing the 6-31G(d,p) basis set for all atoms.[4-9] Natural orbital occupation number (NOON)) calculations were done by spin unrestricted UCAM-B3LYP/6-31G(d,p) method and the diradical character (y_0) was calculated according to Yamaguchi's scheme: $y_0 = 1 − (2T/(1 + T^2))$, and $T = (n_{HOMO} − n_{LUMO})/2$ (n_{HOMO} is the occupation number of the HOMO, n_{LUMO} is the occupation number of the LUMO).[10-11] ACID plot was calculated by using the method developed by Herges.[12] NICS values were calculated using the standard GIAO (GIAO=NMR)[13-14] at the level of B3LYP/6-31G(d,p). The iso-chemical shielding surface (ICSS)[15-16] calculations were carried out to analyze two-dimensional nucleus induced chemical shifts (2D-NICS) along the XY plane.

## 1.4 X-ray crystallographic data

Crystallographic data for compound 7

Single crystal of compound **7** (CCDC No. 2327038) was obtained through slow diffusion of acetonitrile to the toluene solution. CheckCif report for compound **7** has no A or B level alerts were found (Supplementary Fig. 22 and Supplementary Table 17).

Crystallographic data for compound 1

Single crystal of compound **1** (CCDC No. 2337978) was obtained through slow diffusion of acetonitrile to the toluene solution. CheckCif report for compound **1** has no A or B level alerts were found (Supplementary Fig. 23 and Supplementary Table 18).
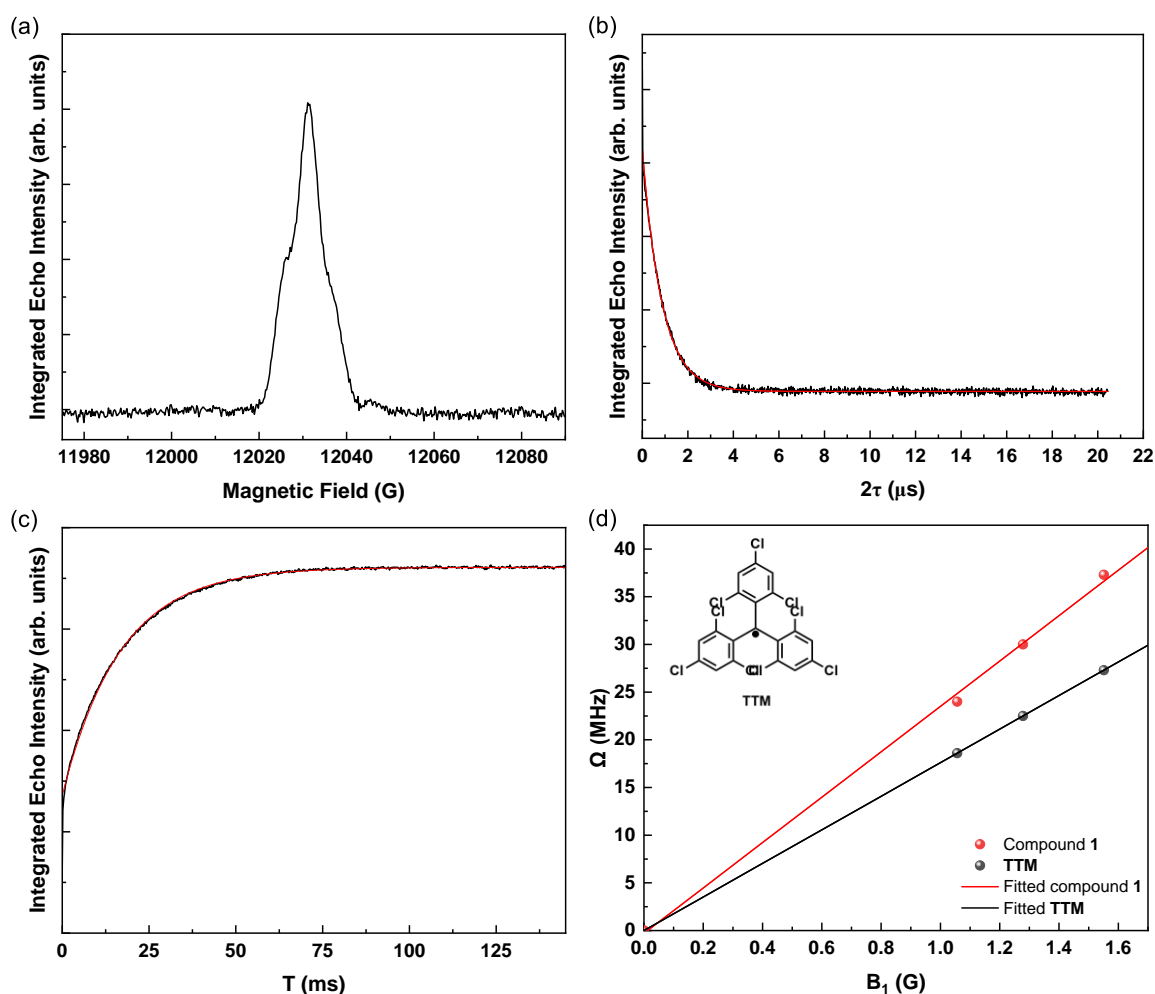
2. Supplementary Figures
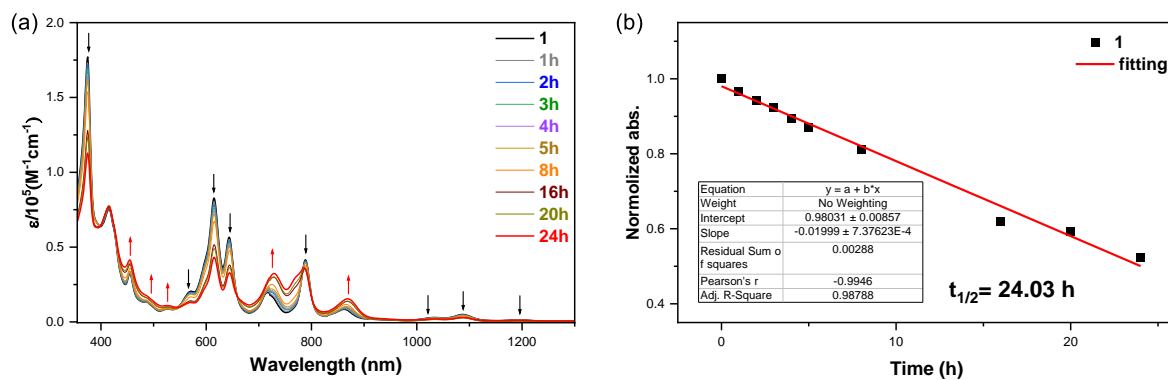
Supplementary Fig. 1. The half-life of **1**. (a) Absorption spectra of **1** in CCl$_4$ recorded at different time when exposure to ambient air and light conditions; (b) plot of the absorbance at 617 nm with time and the half-life time was estimated to be 24.03 h.
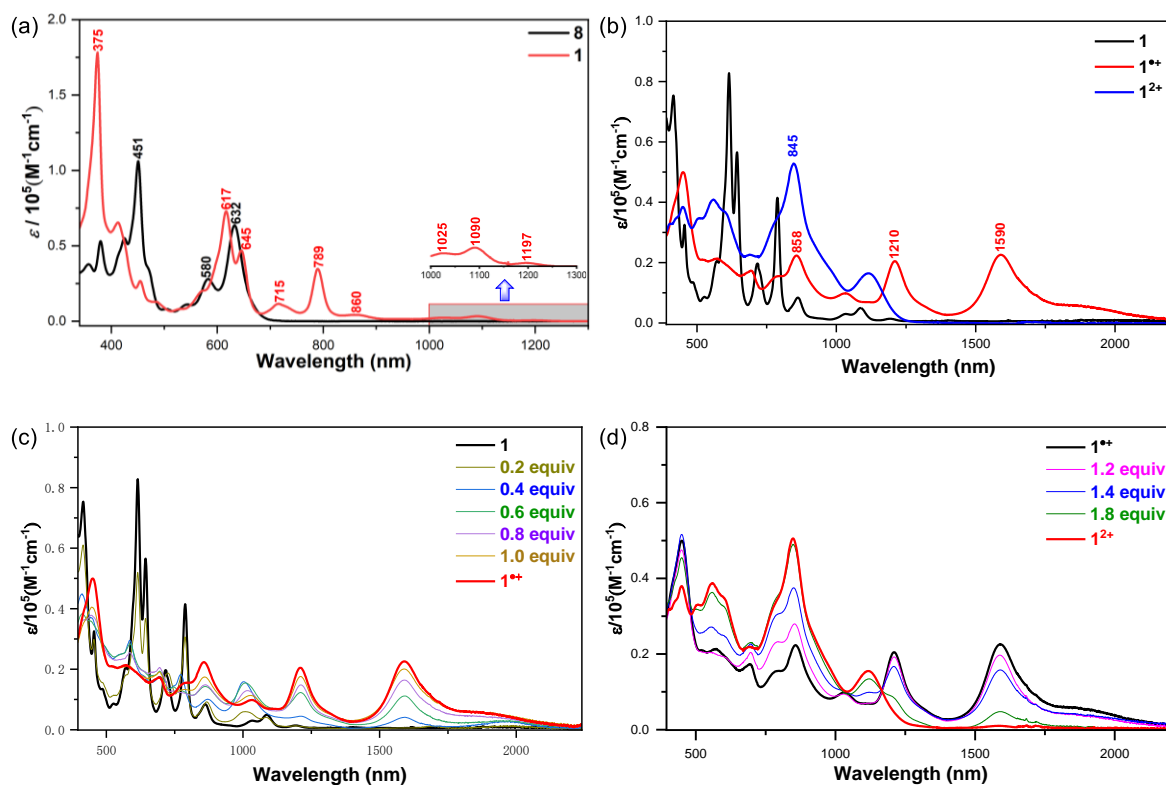
Supplementary Fig. 2. Changes in cationic optical properties of **1**. (a) UV-vis-NIR absorption spectra of compound **8** and **1** upon titration in dry CCl$_4$; (b) UV-vis-NIR absorption spectra of **1**, **1**$^{\bullet+}$ and **1**$^{2+}$ upon titration with NO•SbF$_6$ in dry CCl$_4$; (c) change of the absorption spectrum from neutral to radical cation; (d) change of the absorption spectrum from radical cation to dication.
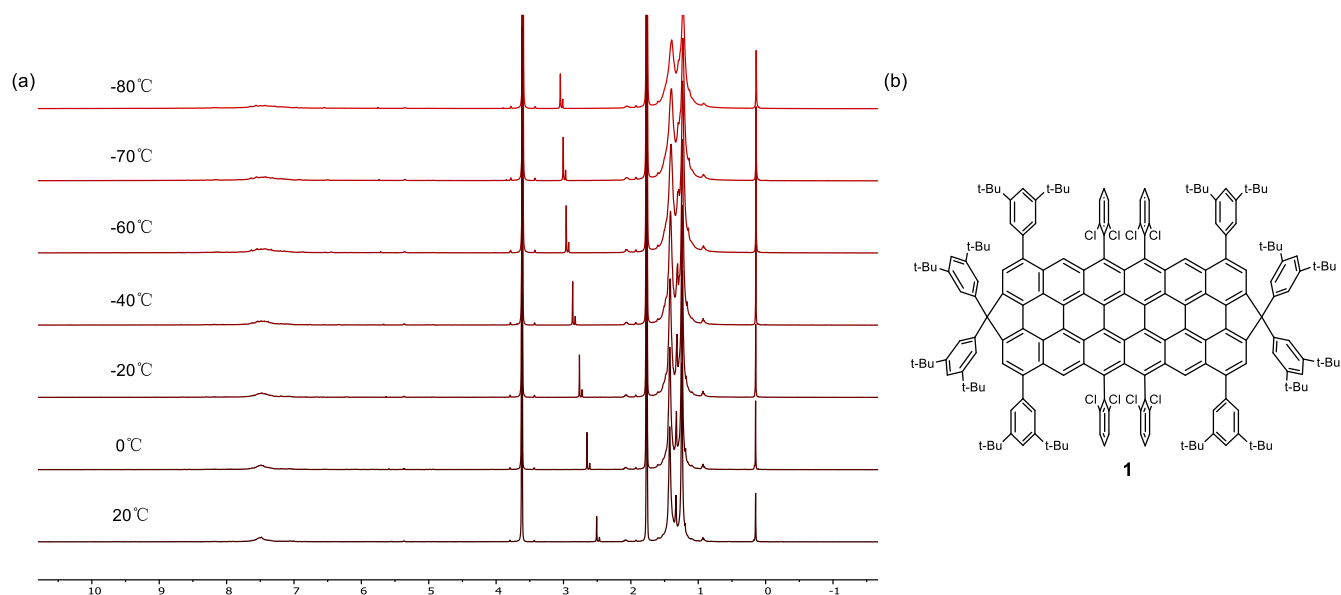
Supplementary Fig. 3. The spectra of compound **1**. (a) VT ^{1}H NMR spectra of compound **1** in d_8-THF (400 MHz). (b) The corresponding structure diagram of compound **1**. (Due to the restricted rotation of the 2,6-dichlorolphenyl substituents and 3,5-di-tert-butylbenzene substituent in **1,** the broadening induced by the thermally populated paramagnetic species, the ^{1}H NMR signals are quite weak and complicated.)

Supplementary Fig. 4. The spin-lattice relaxation time (T1) and spin coherence time (Tm) of **1**. (a) Echo-detected field-swept spectrum (EDFS) for 1 indicated that the applied field of 12031 G with a microwave frequency of 33.720742 GHz gave the largest intensity spin echo. (b) Integrated echo intensity as a function of delay time (2τ) for 1 at 70 K with graphical depiction of Hahn-echo pulse sequence. The red line is a best fit to a stretched exponential decay with $T_m = 0.85$ μs. (c) Integrated echo intensity as a function of delay time (T) for 1 at 70 K with graphical depiction of Hahn-echo pulse sequence. The red line is a best fit to a stretched exponential decay with $T_1 = 16.7$ ms. (d) Corresponding dependence of the Rabi frequency (Ω) on the **B₁** field. Key: standard radical TTM (black line), 1 (red line).
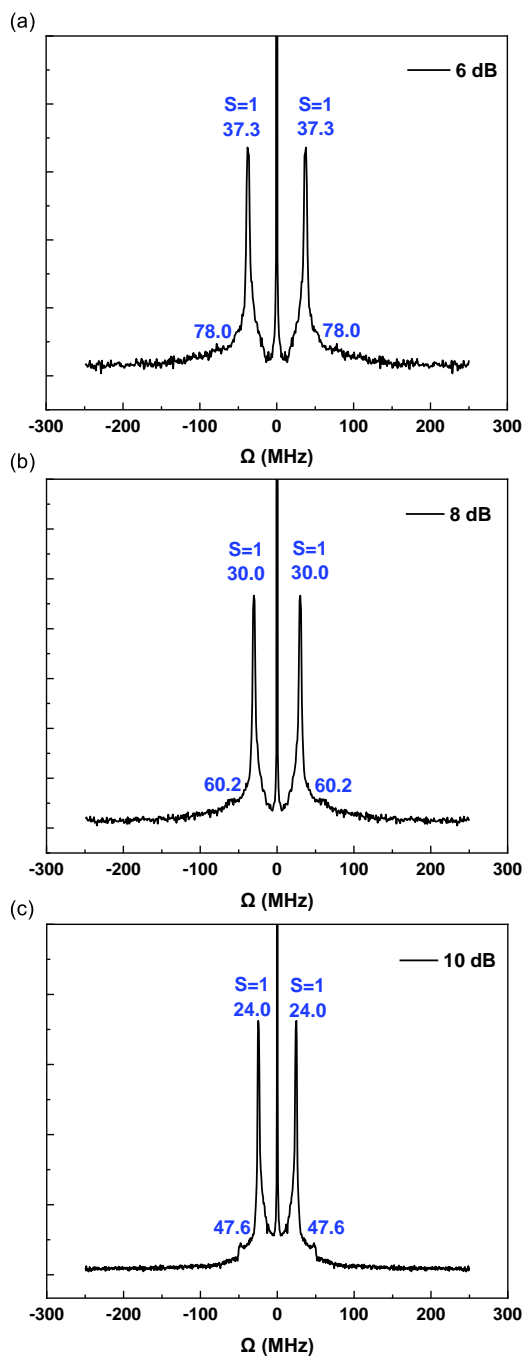
Supplementary Fig. 5. The nutation pulses were applied in three distinctive microwave powers (6 (a), 8 (b), and 10 (c) dB) at 70 K so as to vary the **B₁** field, which are assigned to the triplet state of **1** and a small amount of doublet impurity, respectively.
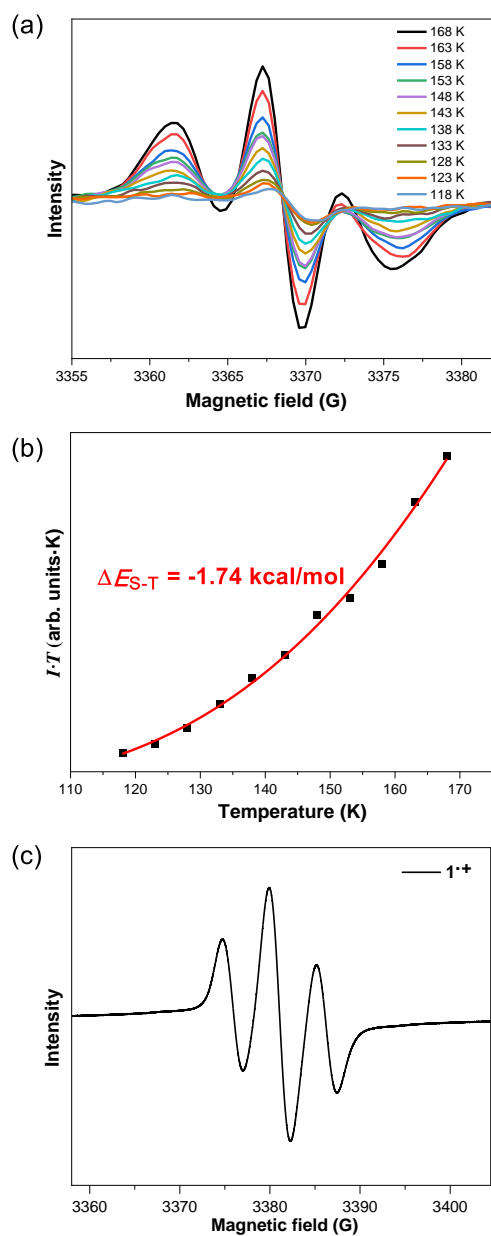
Supplementary Fig. 6. The EPR of **1** or **1**$^{·+}$ in solution. (a) Variable-temperature EPR spectra of compound **1** in frozen toluene solution. (b) Fitted $I \times T - T$ curve of compound **1** in frozen toluene solutions. (c) EPR spectra of compound **1**$^{·+}$ in DCM solutions.

SOMO-α

SOMO-β
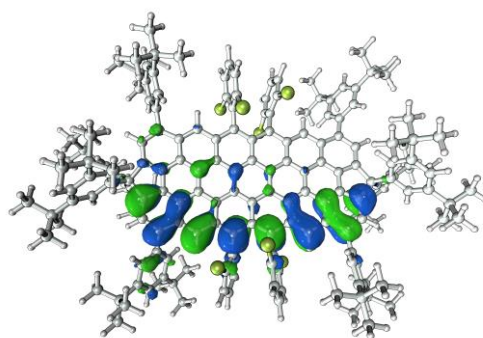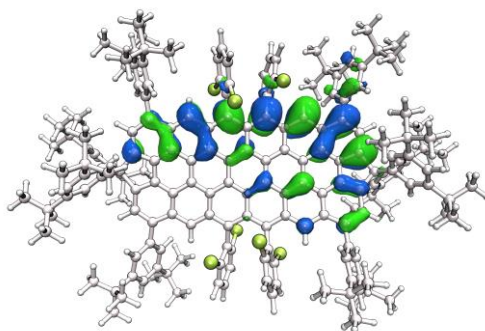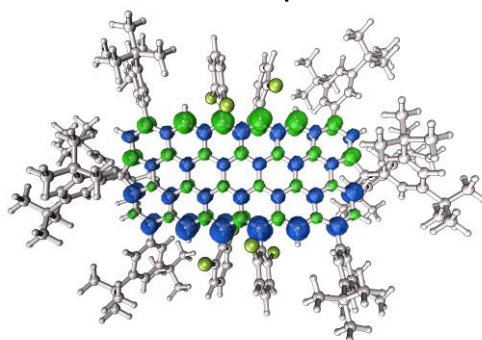
Spin density(SB)

Supplementary Fig. 7. Calculated (UB3LYP/6-31G(d,p)) molecular orbital profiles of α and β spins, and the spin density distribution of the singlet biradical (SB) state of **1**.
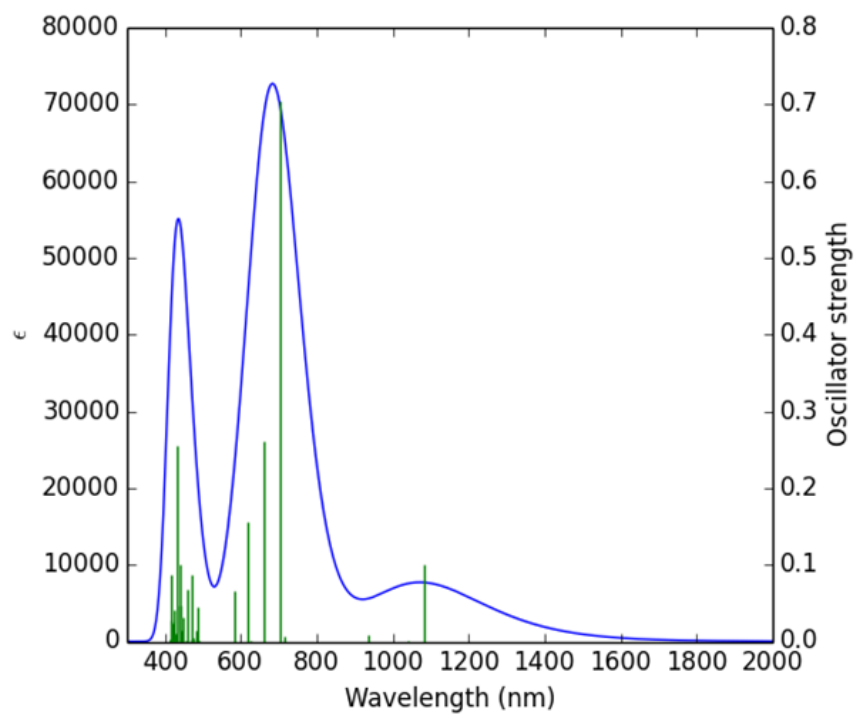
Supplementary Fig. 8. TD DFT (UB3LYP/6-31G(d,p)) simulated spectra of **1**. The calculation method is shown in the table below.
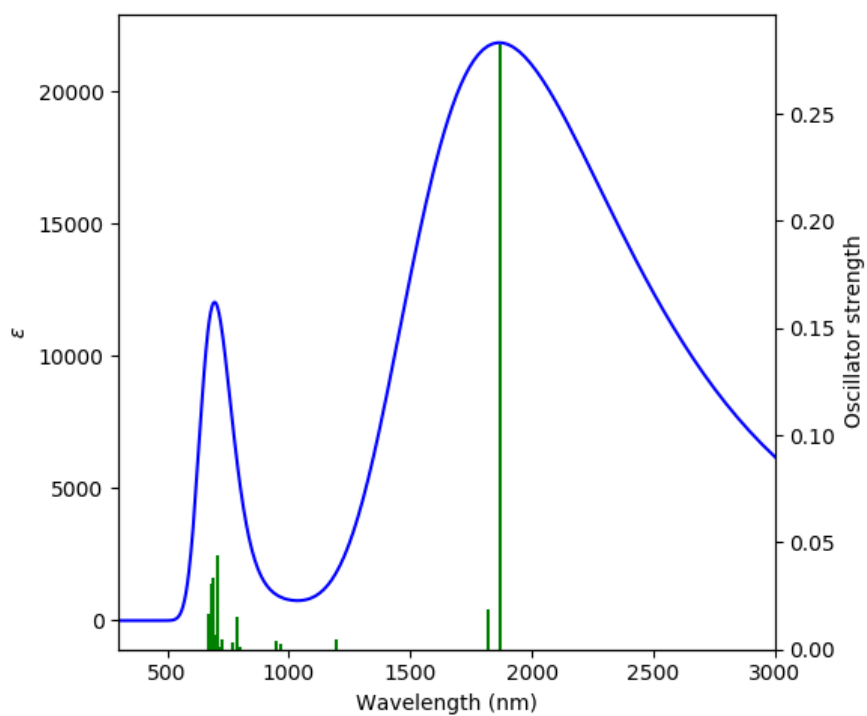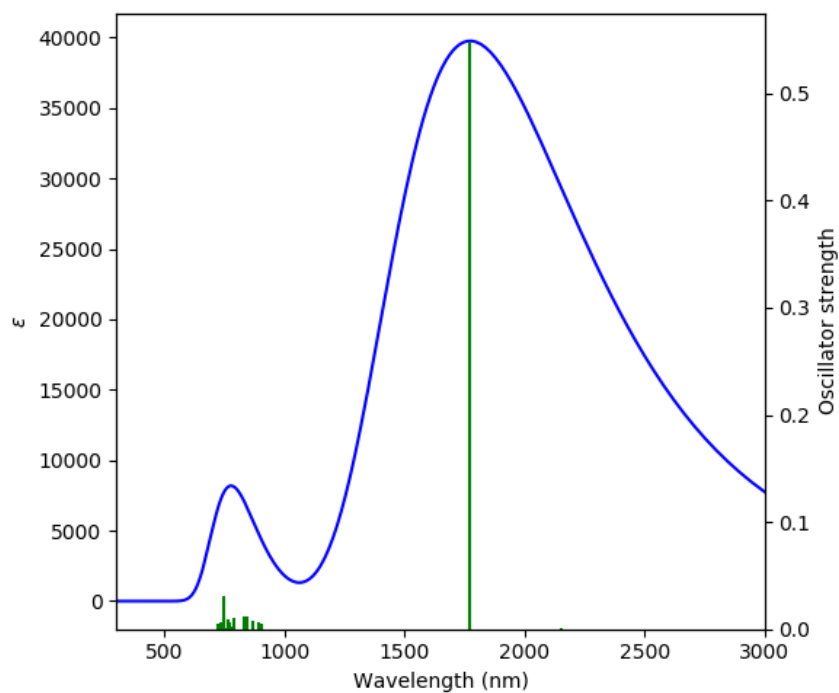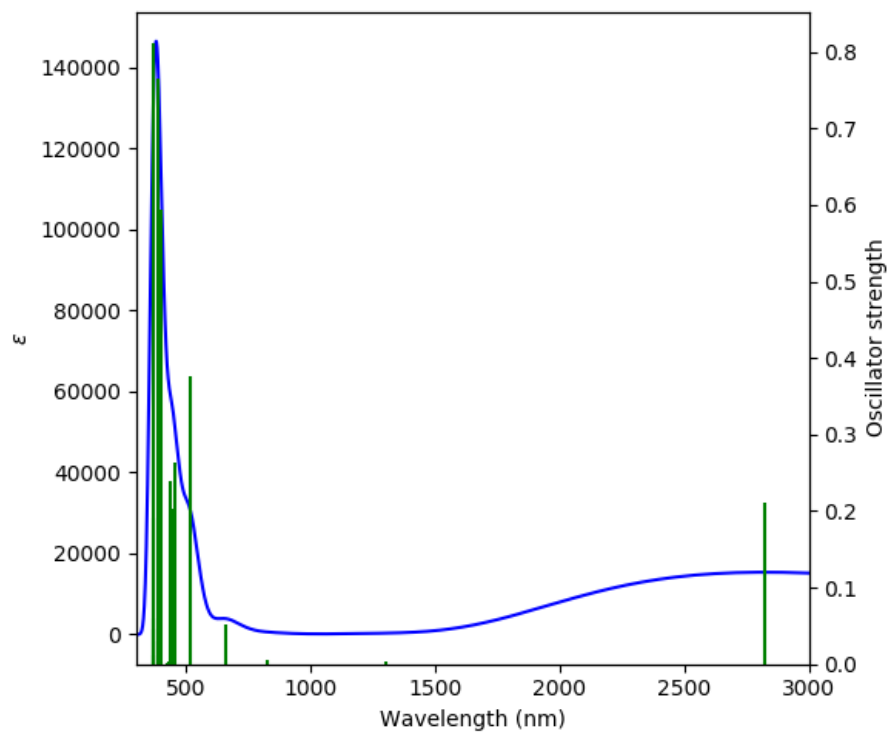
Supplementary Fig. 9. TD-DFT (UB3LYP/6-31G(d,p)) simulated spectra of **1·⁺**. The calculation method is shown in the table below.
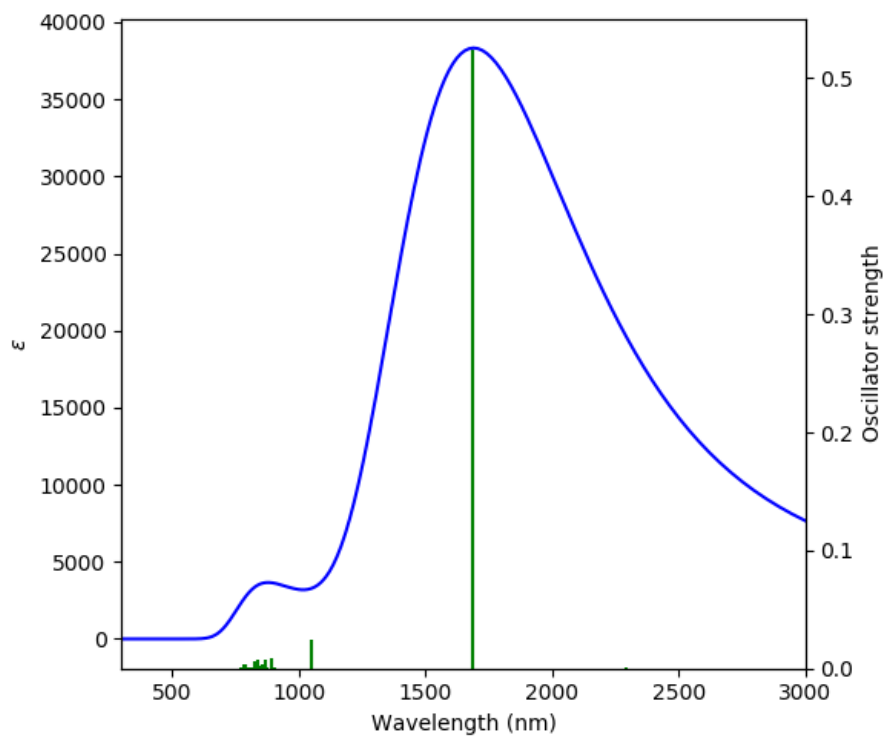
Supplementary Fig. 10. TD-DFT (UB3LYP/6-31G(d,p)) simulated spectra of 1^{2+}. The calculation method is shown in the table below.
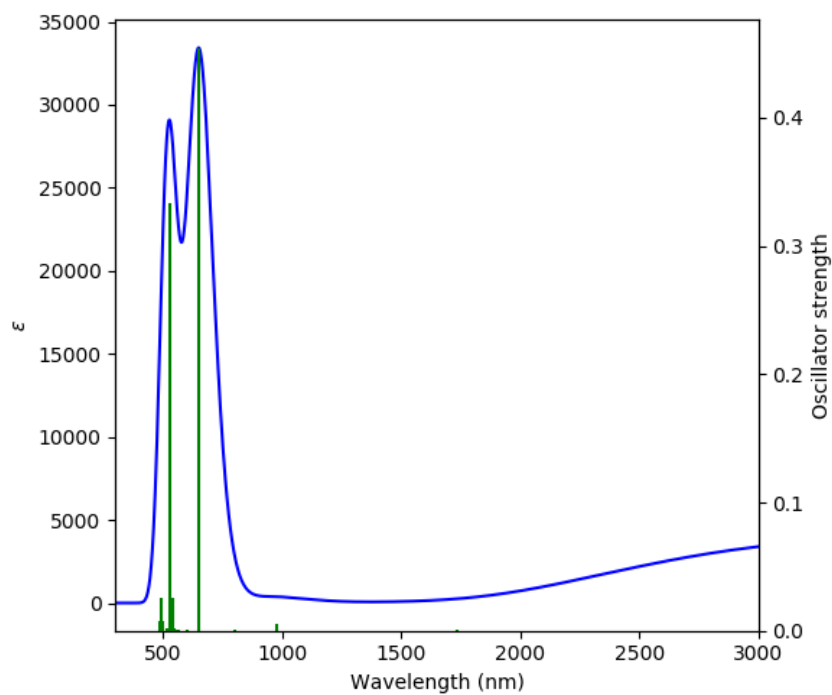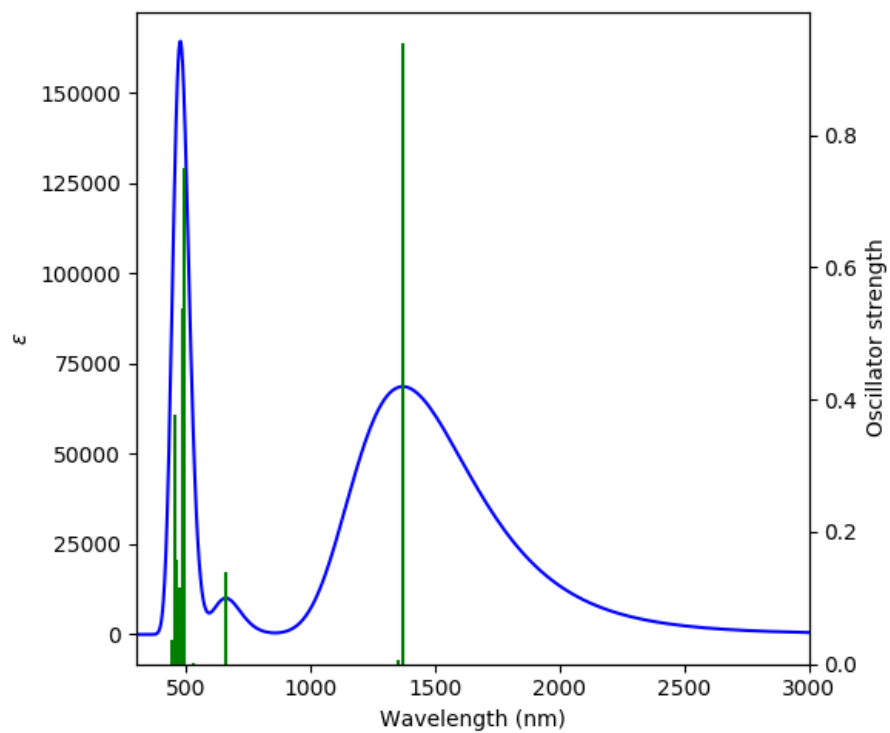
Supplementary Fig. 11. TD-DFT (RB3LYP/6-31G(d,p)) simulated spectra of **1**. The calculation method is shown in the table below.
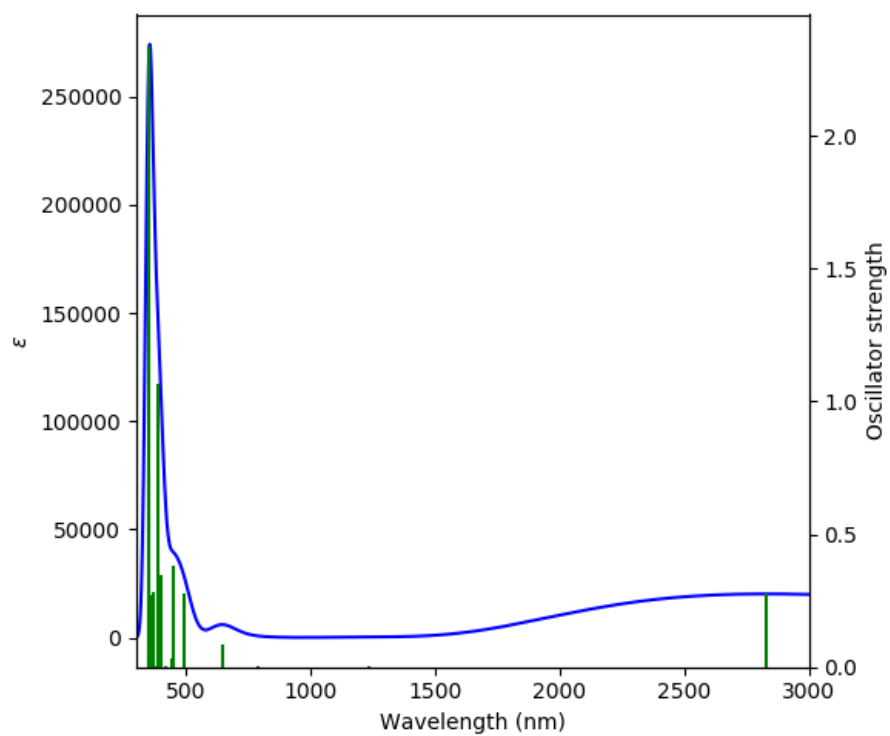
Supplementary Fig. 12. TD-DFT (RB3LYP/6-31G(d,p)) simulated spectra of **1^{2+}**. The calculation method is shown in the table below.
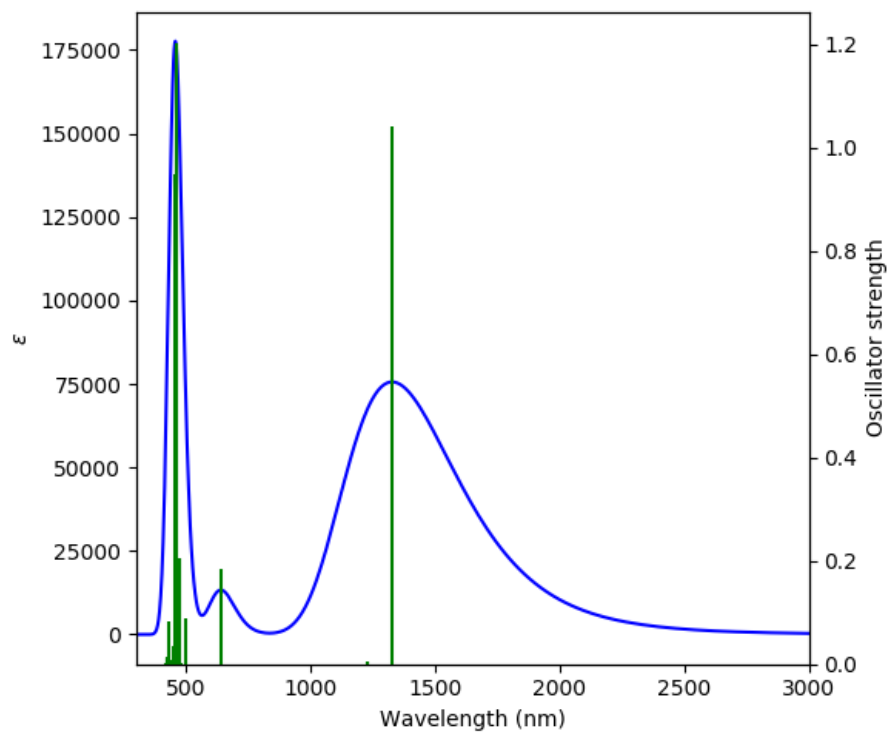
Supplementary Fig. 13. TD-DFT (RCAM-B3LYP/6-31G(d,p)) simulated spectra of **1**. The calculation method is shown in the table below.
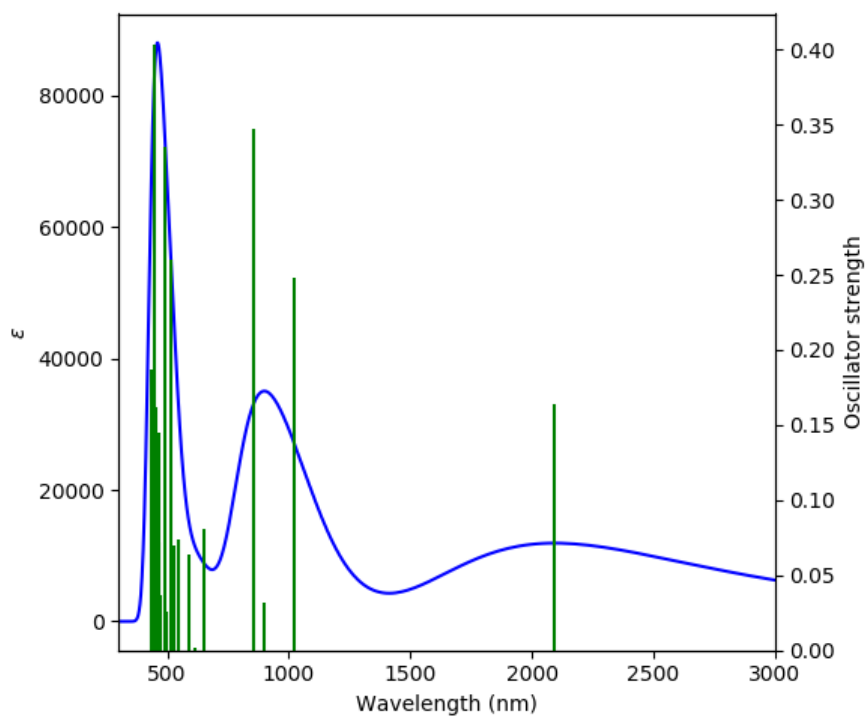
Supplementary Fig. 14. TD-DFT (RCAM-B3LYP/6-31G(d,p)) simulated spectra of 1^{2+}. The calculation method is shown in the table below.
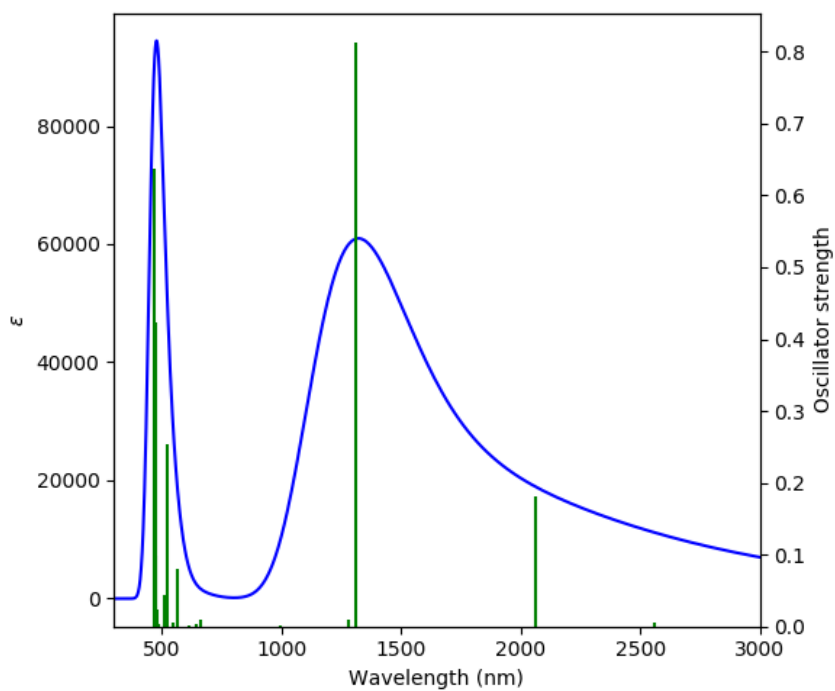
Supplementary Fig. 15. TD-DFT (RωB97XD/6-31G(d,p)) simulated spectra of **1**. The calculation method is shown in the table below.

Supplementary Fig. 16. TD-DFT (RωB97XD/6-31G(d,p)) simulated spectra of **1²⁺**. The calculation method is shown in the table below.

Supplementary Fig. 17. TD-DFT (UCAM-B3LYP/6-31G(d,p)) simulated spectra of **1**·⁺. The calculation method is shown in the table below.

Supplementary Fig. 18. TD-DFT (UCAM-B3LYP/6-31G(d,p)) simulated spectra of 1^{2+}. The calculation method is shown in the table below.

Supplementary Fig. 19. TD-DFT (UωB97XD/6-31G(d,p)) simulated spectra of **1**. The calculation method is shown in the table below.
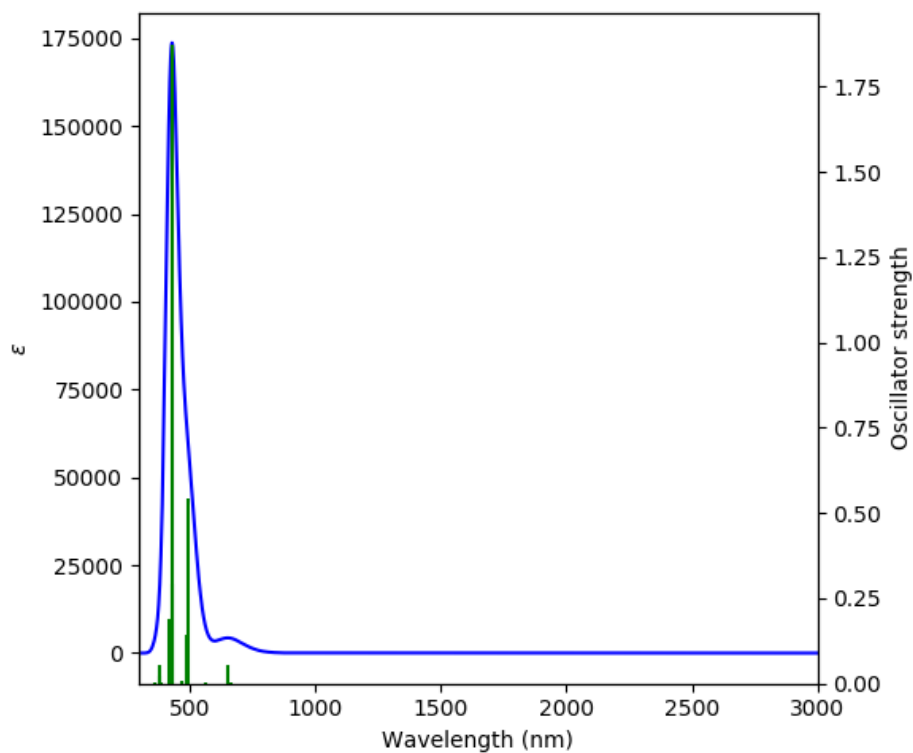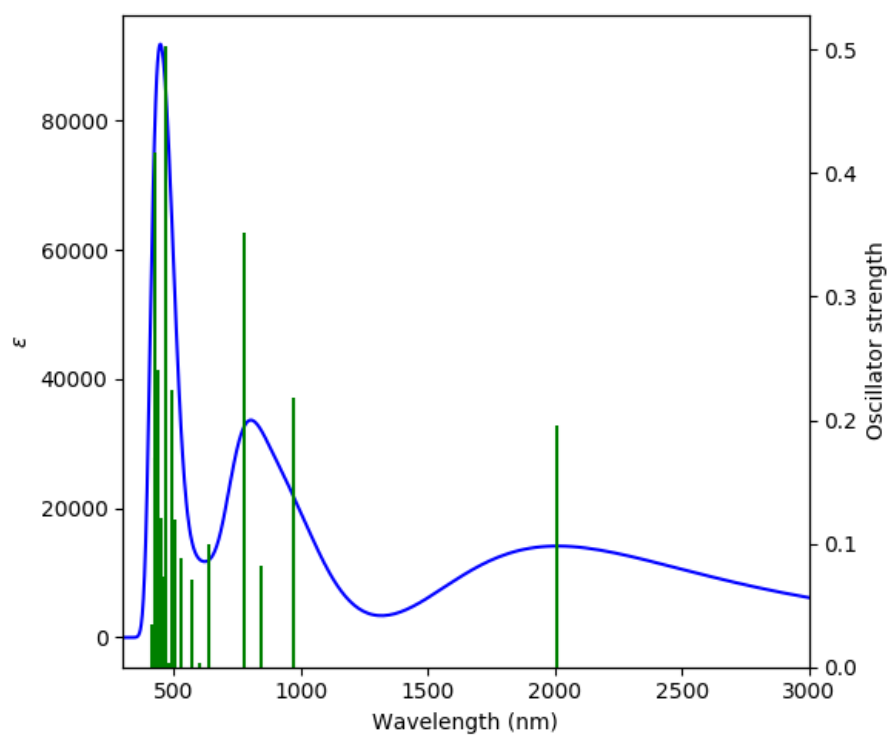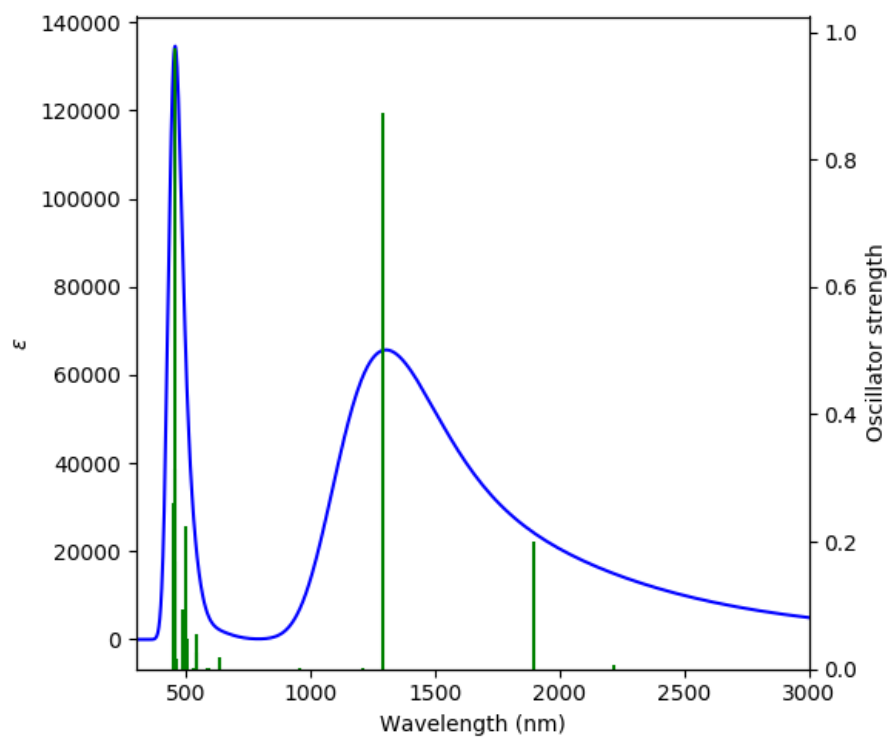
Supplementary Fig. 20. TD-DFT (UωB97XD/6-31G(d,p)) simulated spectra of **1**[.+]. The calculation method is shown in the table below.

Supplementary Fig. 21. TD-DFT (UωB97XD/6-31G(d,p)) simulated spectra of **1²⁺**. The calculation method is shown in the table below.
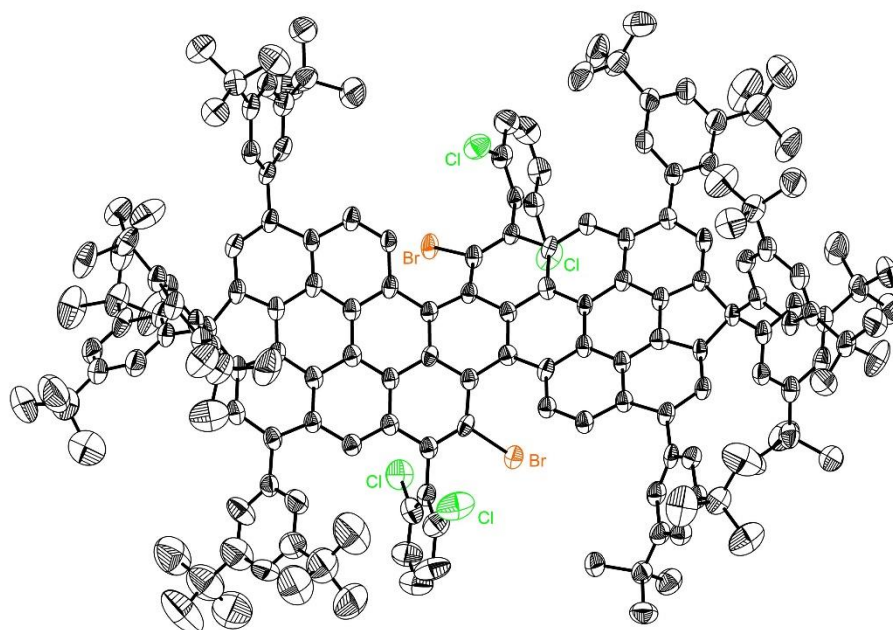
(a) Top view　　　　　　　　　　　　　　　**(b) Side view**
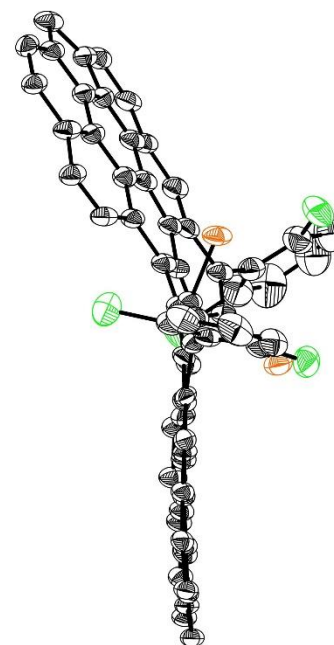
Supplementary Fig. 22. Solid-state structure of **7** shown at the 50% probability level(CCDC NO. 2327038). (a) Top view of X-ray crystallographic structure of compound **7**. (b) side view of X-ray crystallographic structure of compound **7**; Hydrogen atoms, solvent molecules and any disorders are omitted for clarity.

(a) Top view

(b) Side view
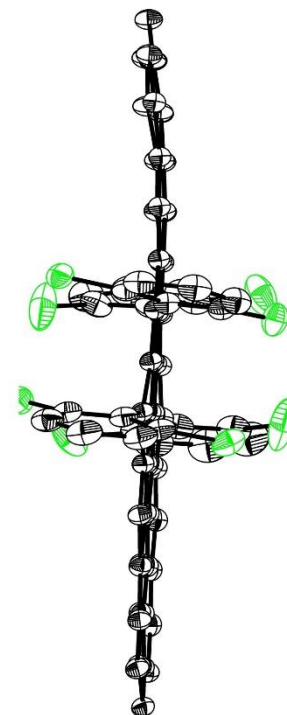
Supplementary Fig. 23. Solid-state structure of **1** shown at the 50% probability level (CCDC NO. 2337978). (a) Top view of X-ray crystallo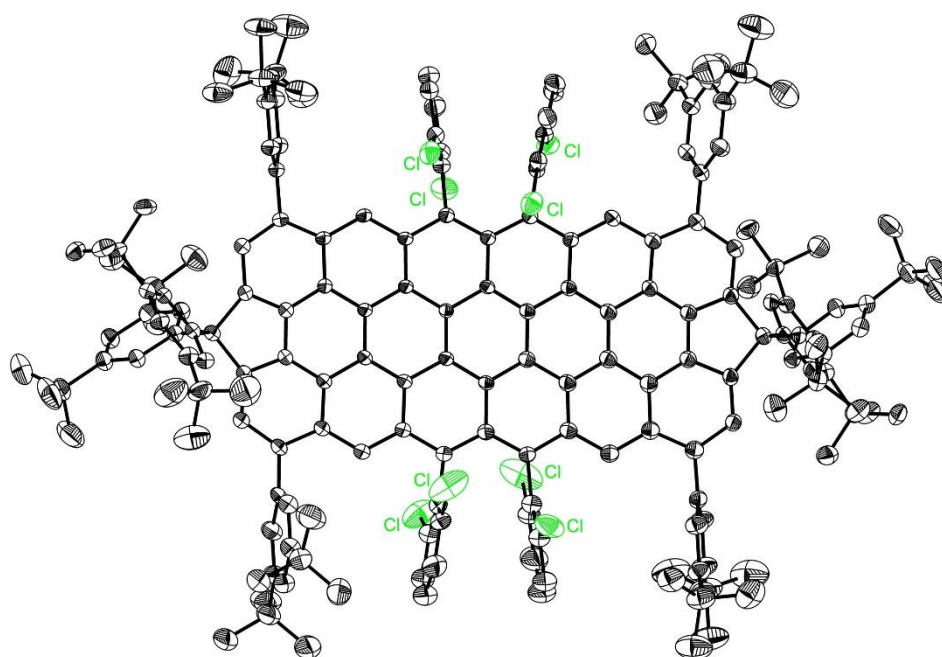graphic structure of compound **1**. (b) side view of X-ray crystallographic structure of compound **1**; Hydrogen atoms, solvent molecules and any disorders are omitted for clarity.
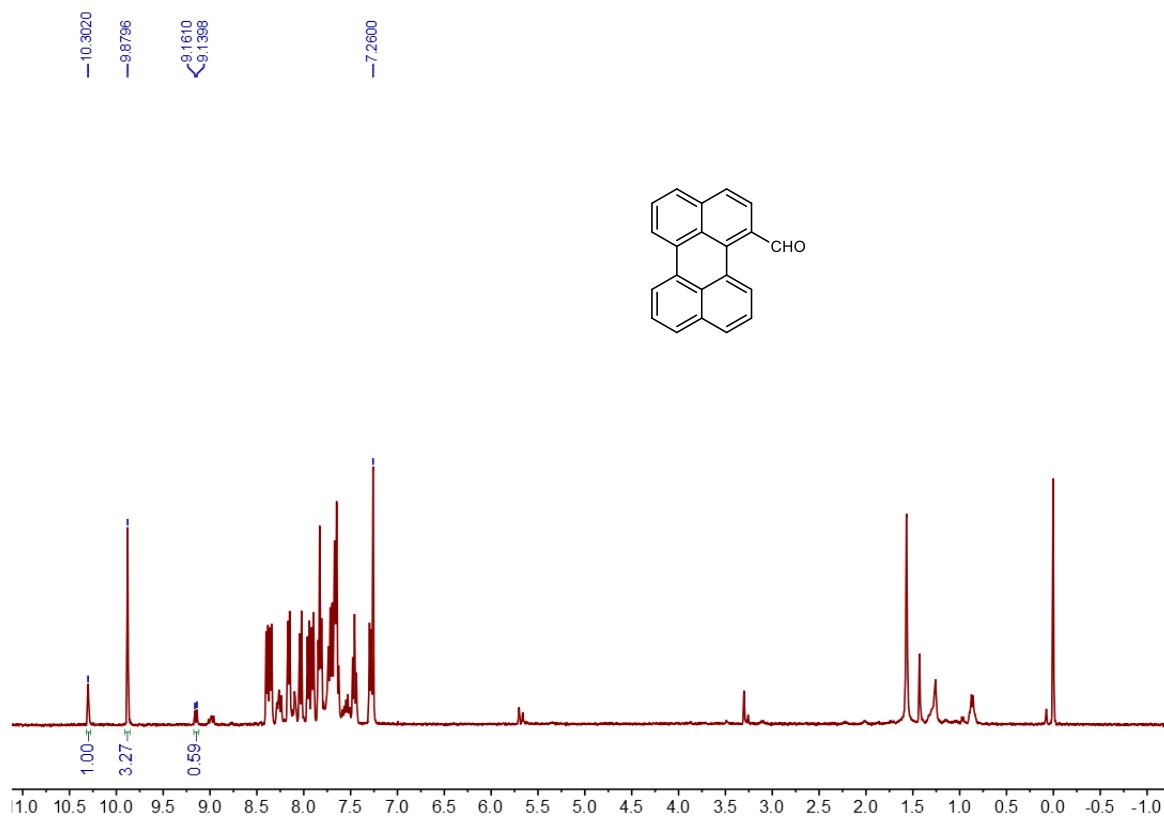
Supplementary Fig. 24. ^{1}H NMR spectrum of perylene-1-carbaldehyde (400 MHz, CDCl$_3$, rt).
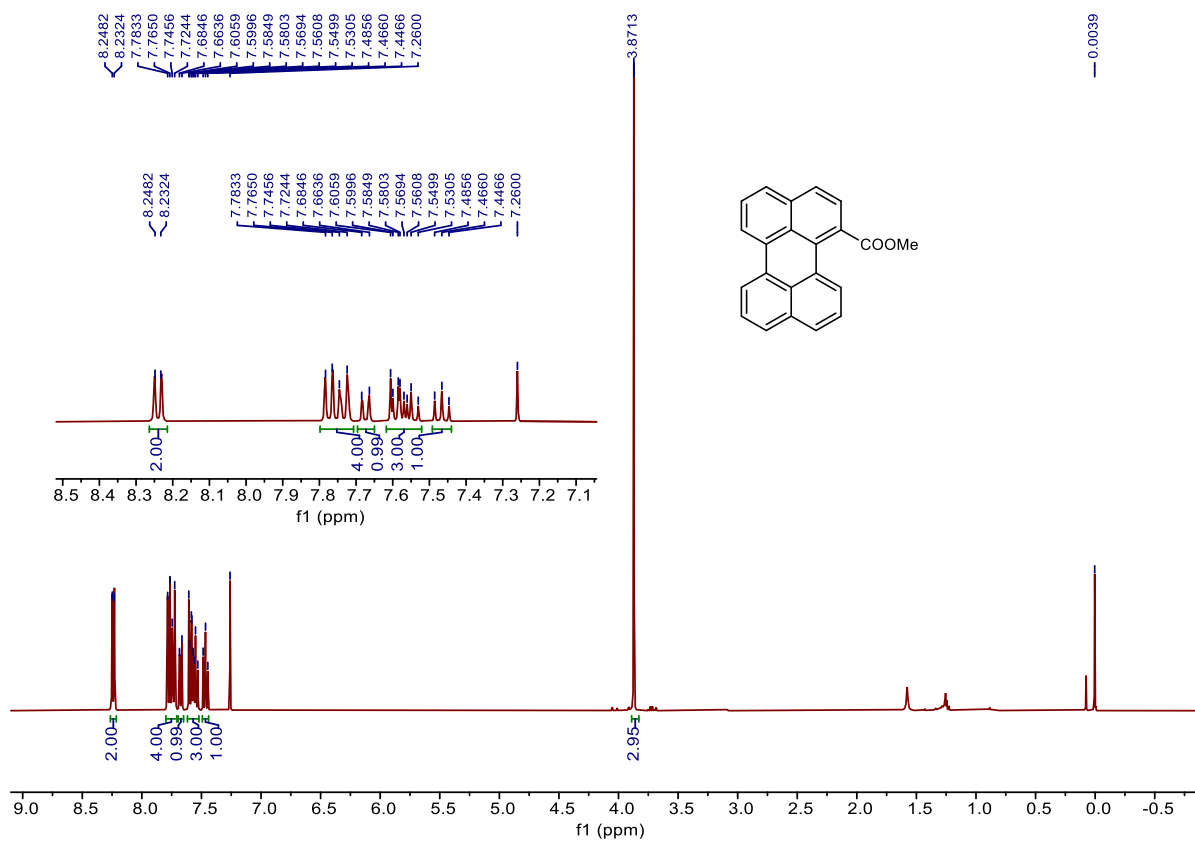
Supplementary Fig. 25. ^{1}H NMR spectrum of methyl perylene-1-carboxylate (400 MHz, CDCl$_3$, rt).
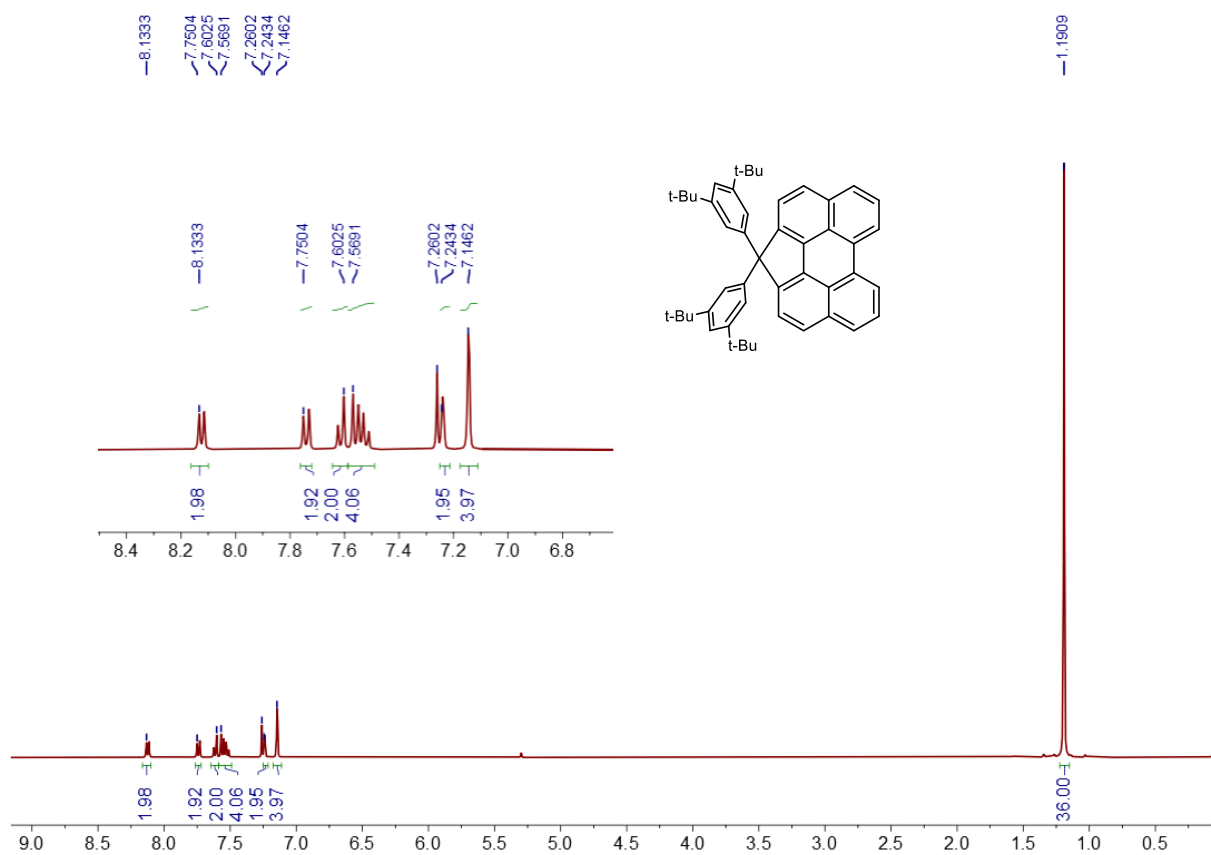
Supplementary Fig. 26. ^{1}H NMR spectrum of 1,1-bis(3,5-di-tert-butylphenyl)-1H-cyclopenta[ghi]perylene (400 MHz, CDCl$_3$, rt).
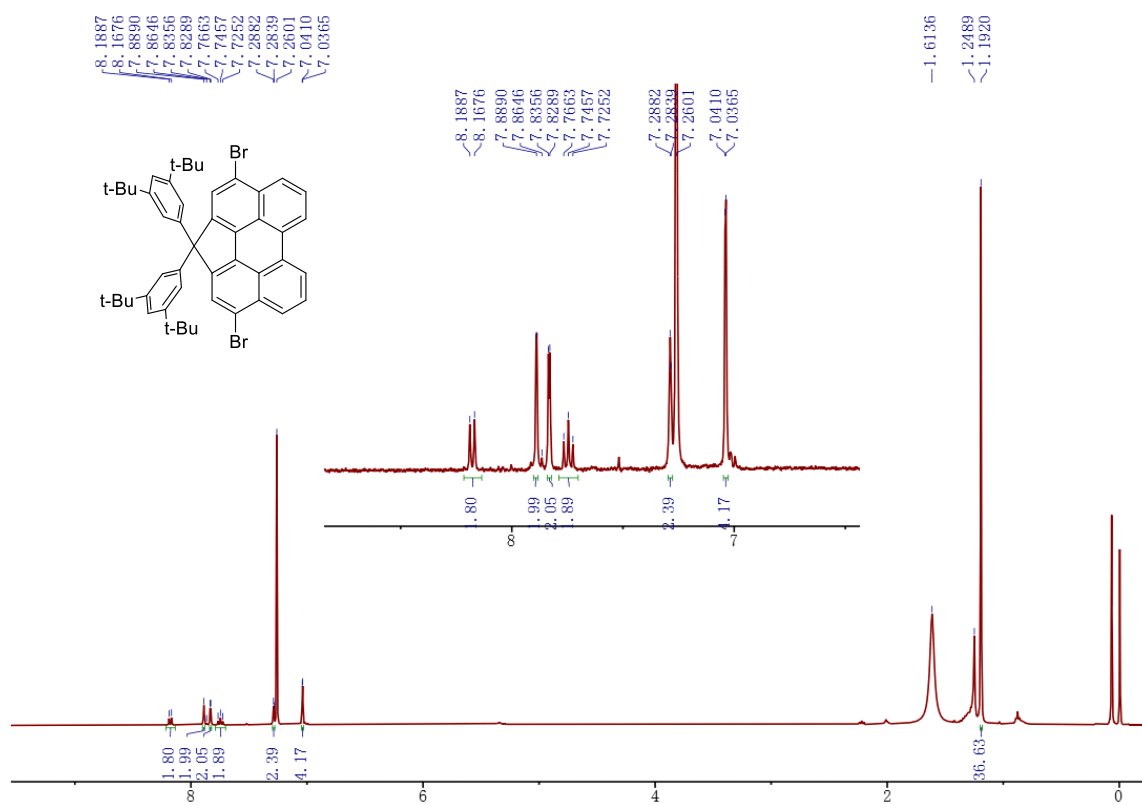
Supplementary Fig. 27. ^{1}H NMR spectrum of 3,10-dibromo-1,1-bis(3,5-di-tert-butylphenyl)-1H-cyclopenta[ghi]perylene (400 MHz, CDCl$_3$, rt).
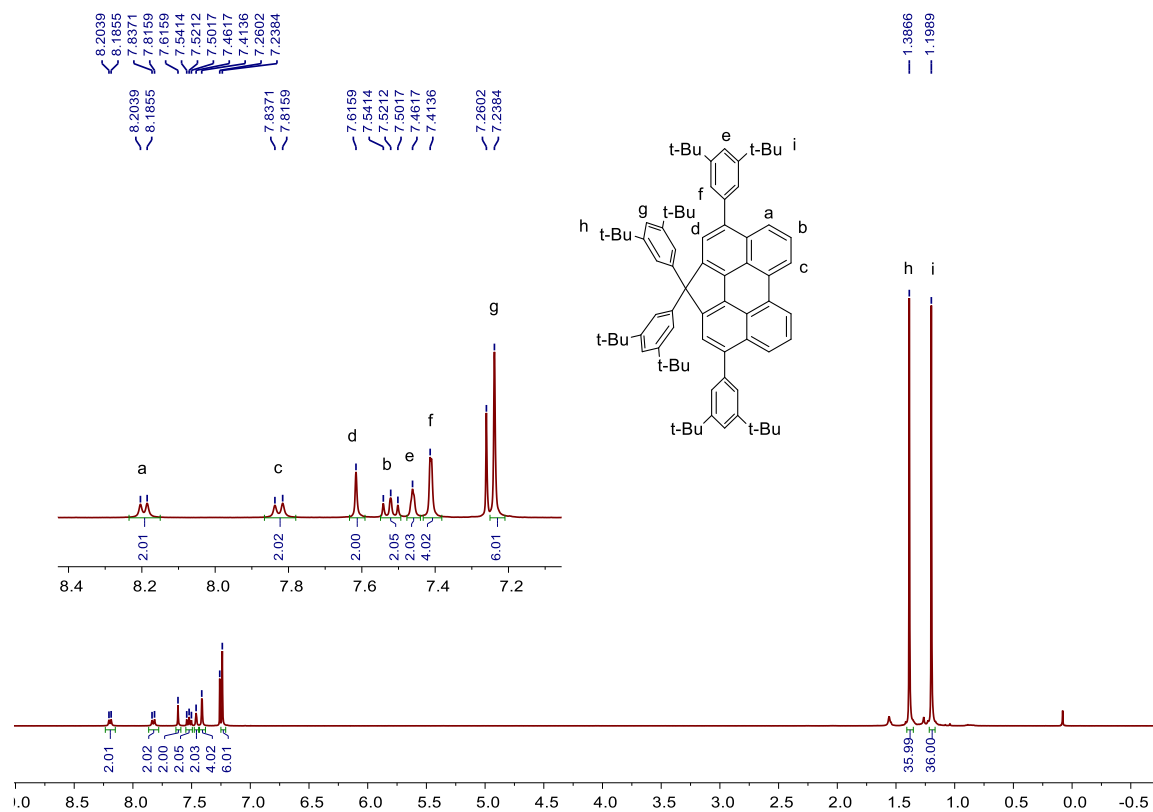
Supplementary Fig. 28. ^{1}H NMR spectrum of compound **2** (400 MHz, CDCl$_3$, rt).
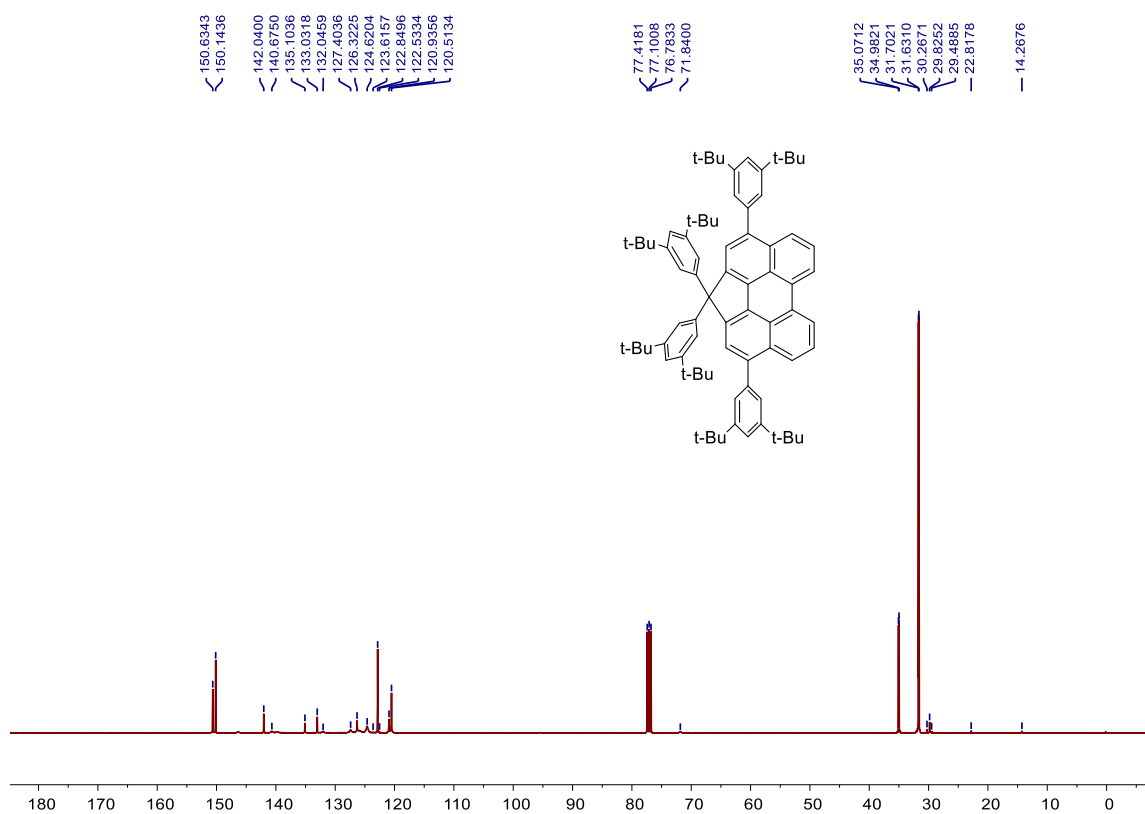
Supplementary Fig. 29. ^{13}C NMR spectrum of compound **2** (125 MHz, CDCl$_3$, rt)
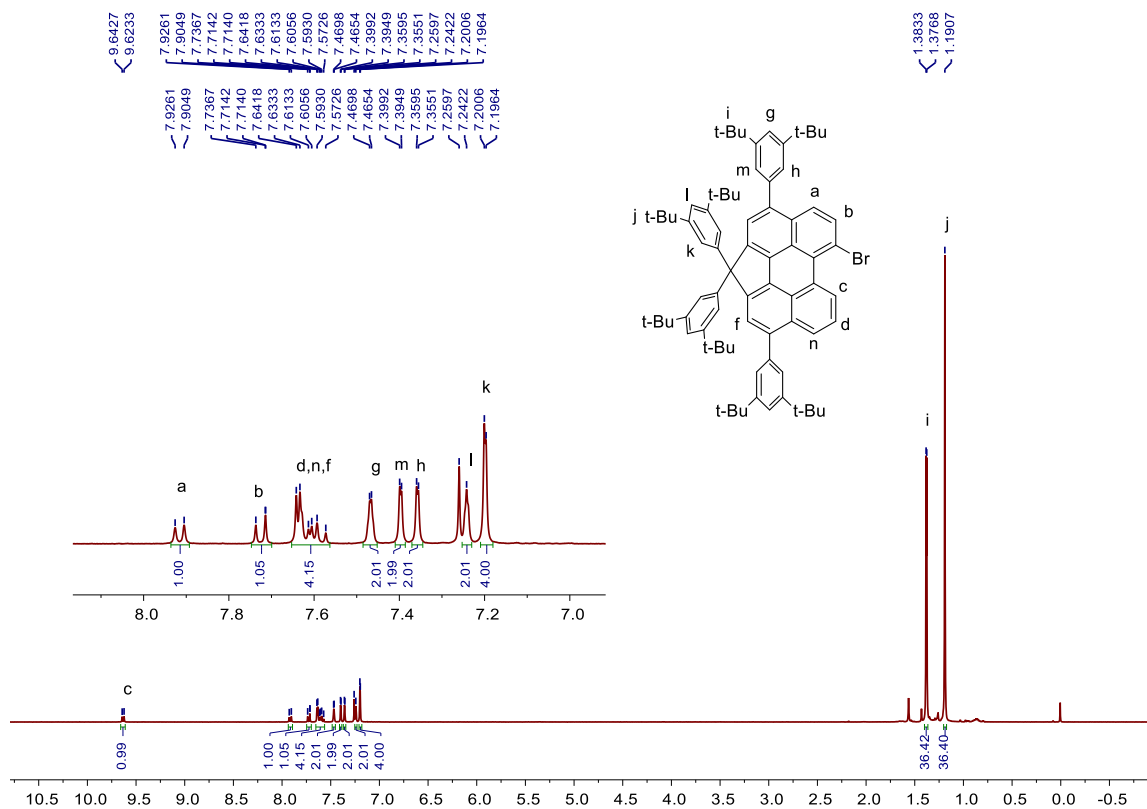
Supplementary Fig. 30. ^{1}H NMR spectrum of compound **3** (400 MHz, CDCl$_3$, rt).
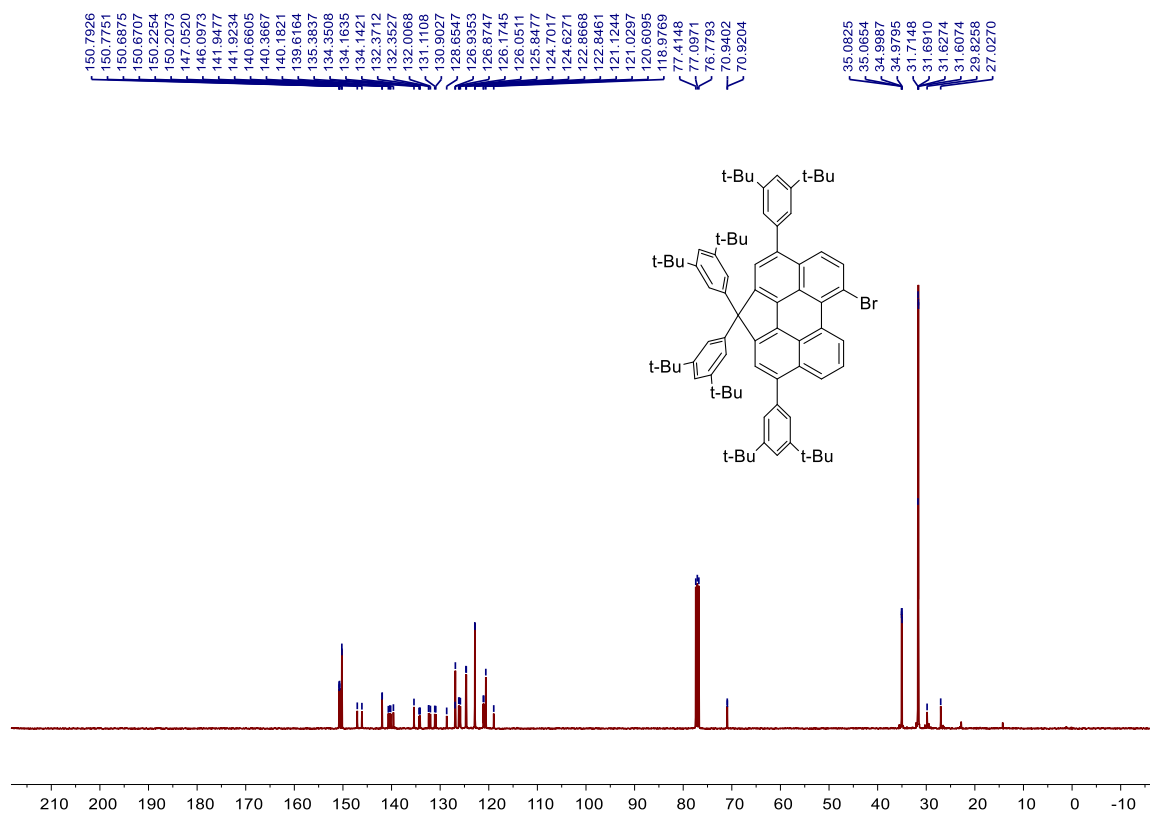
Supplementary Fig. 31. ^{13}C NMR spectrum of compound **3** (125 MHz, CDCl$_3$, rt)
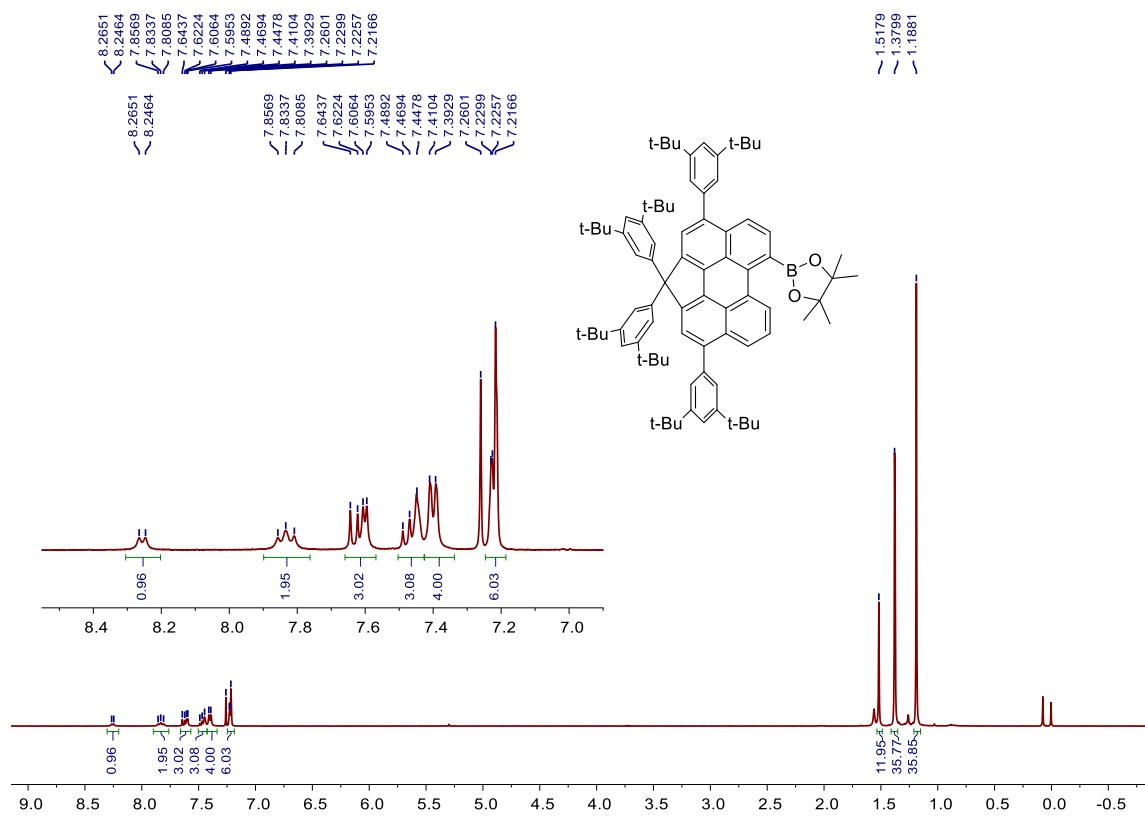
Supplementary Fig. 32. ^{1}H NMR spectrum of compound **4** (400 MHz, CDCl$_3$, rt).
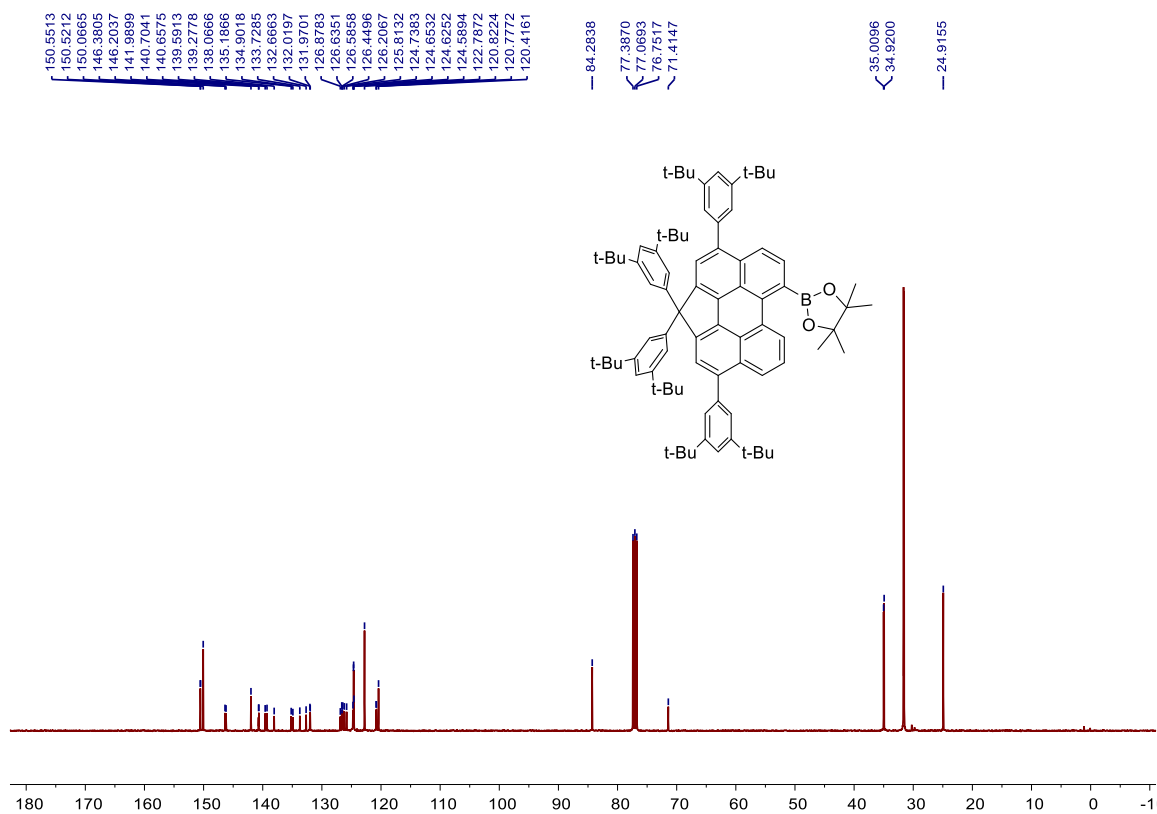
Supplementary Fig. 33. ^{13}C NMR spectrum of compound **4** (125 MHz, CDCl$_3$, rt)
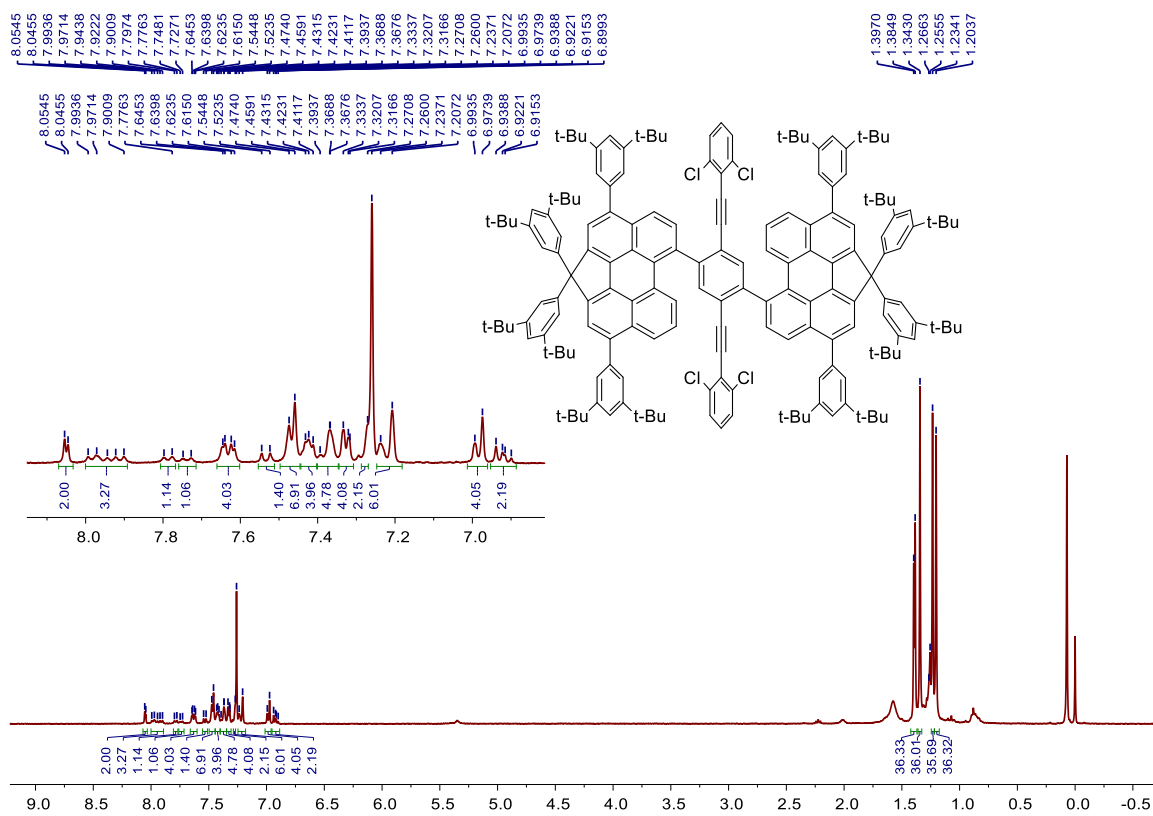
Supplementary Fig. 34. ^{1}H NMR spectrum of compound **6** (400 MHz, CDCl$_3$, rt).
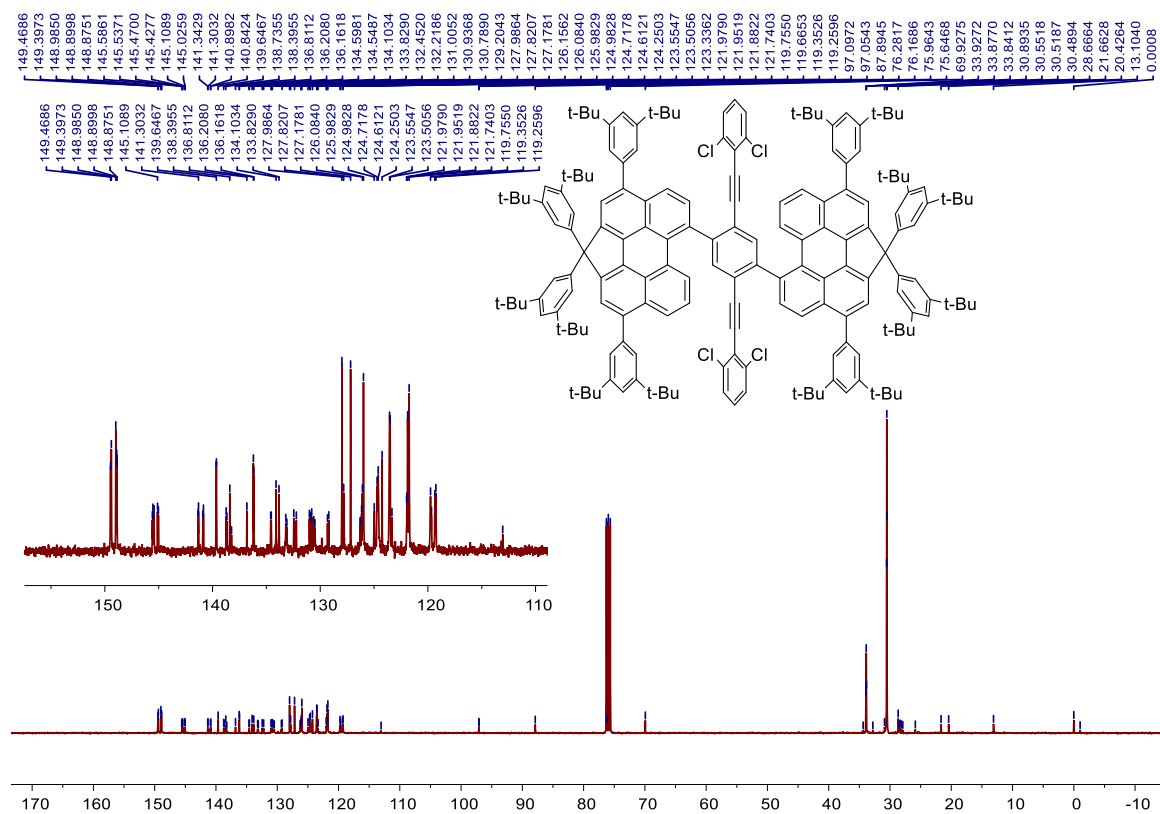
Supplementary Fig. 35. ^{13}C NMR spectrum of compound **6** (125 MHz, CDCl$_3$, rt).
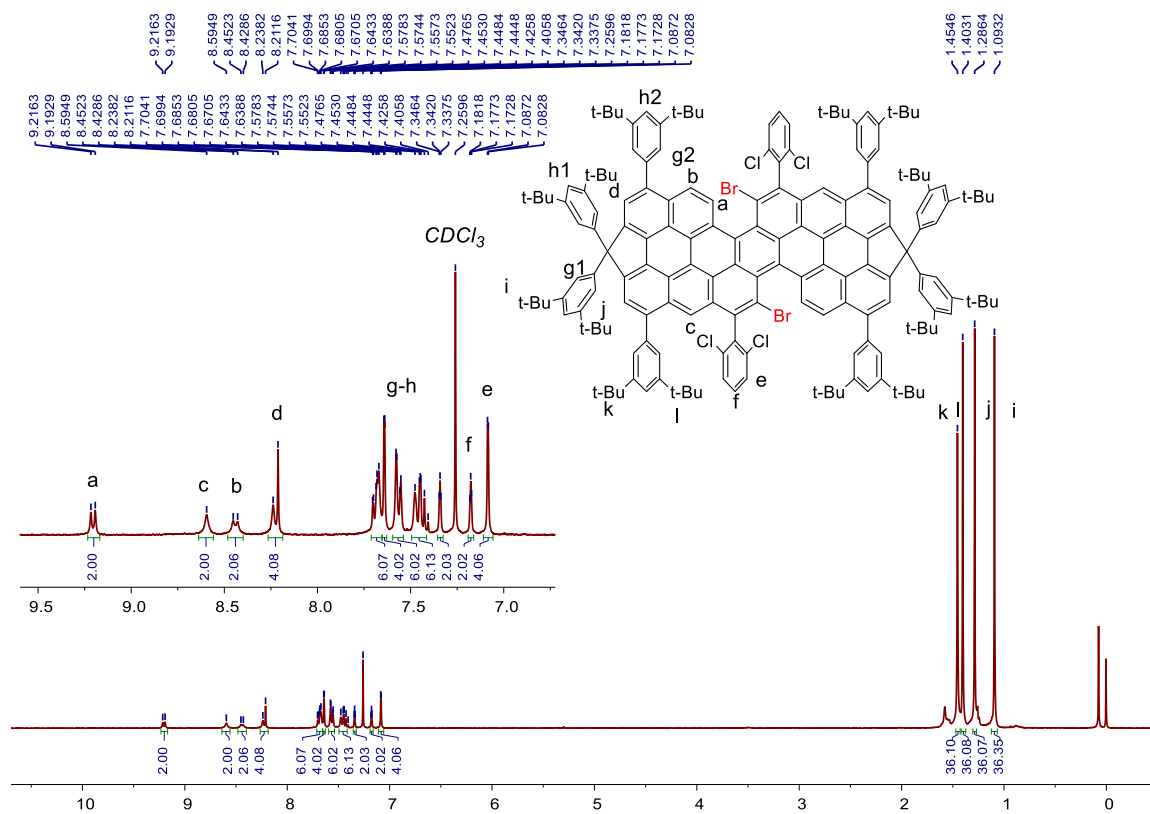
Supplementary Fig. 36. ^{1}H NMR spectrum of compound **7** (400 MHz, CDCl$_3$, rt).
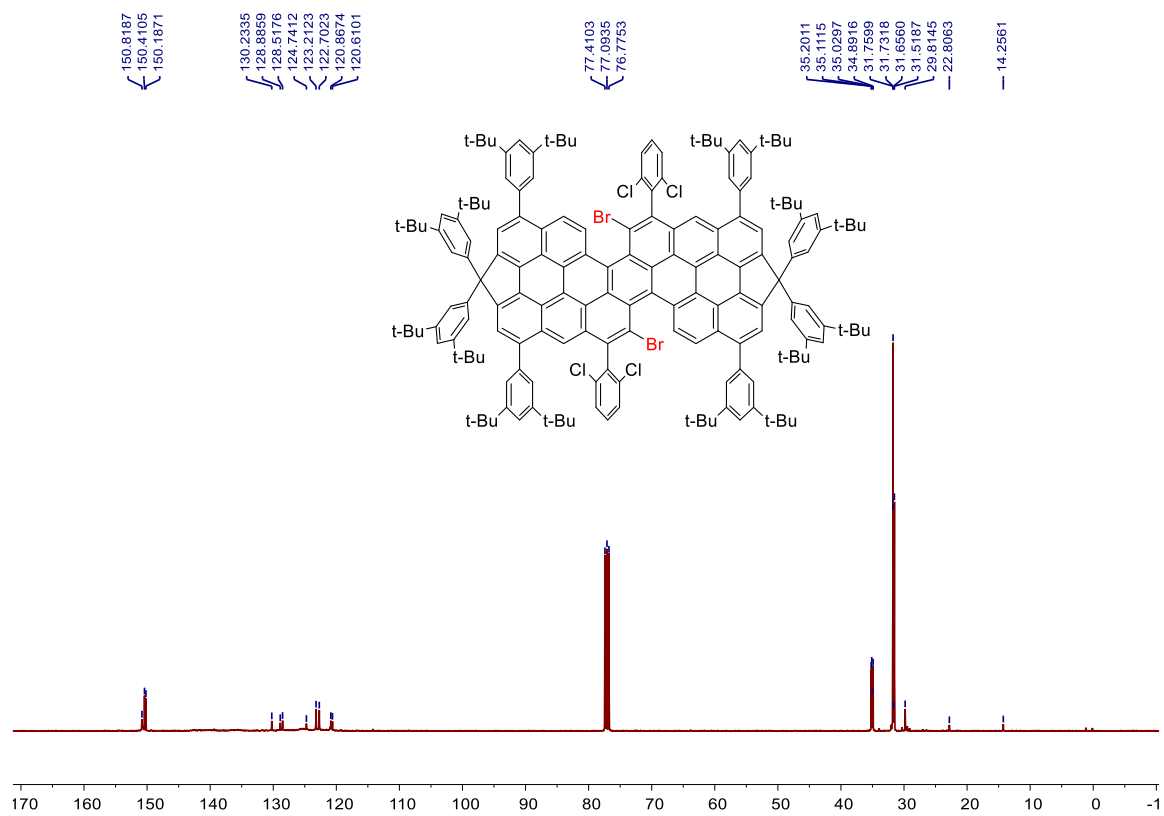
Supplementary Fig. 37. ^{13}C NMR spectrum of compound **7** (125 MHz, CDCl$_3$, rt)

49
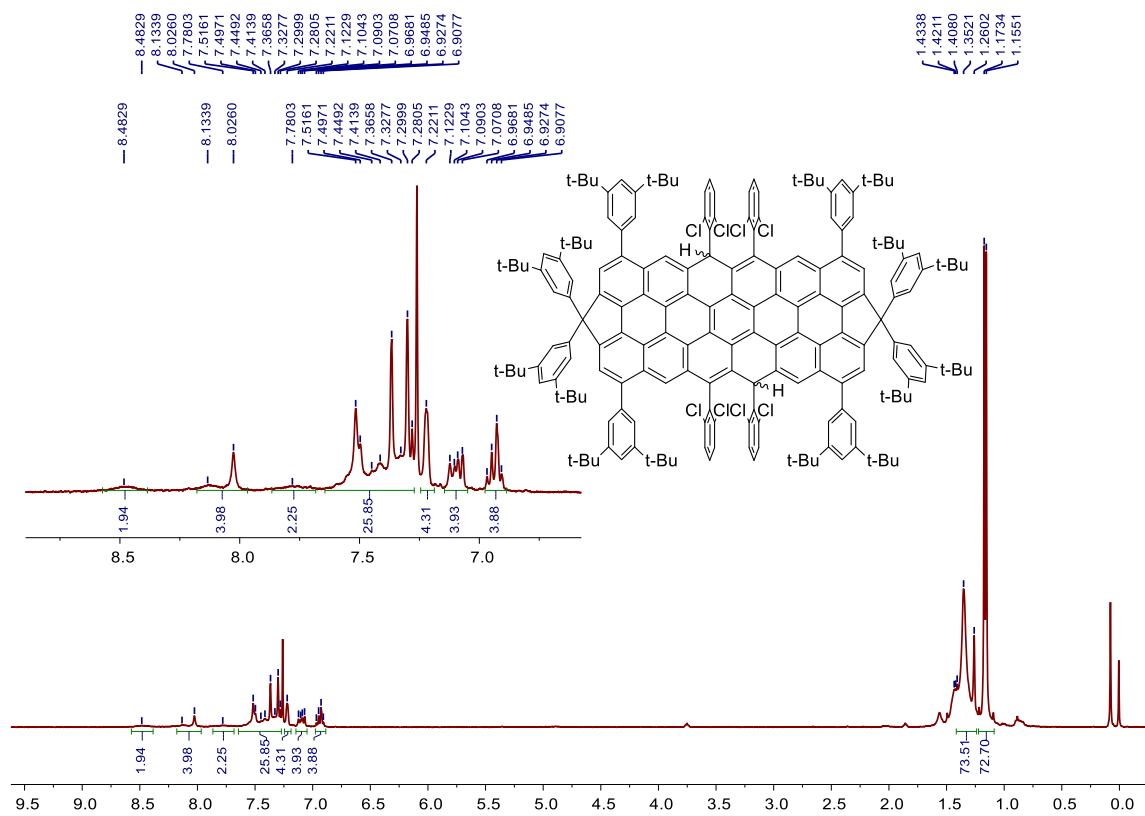
Supplementary Fig. 38. ^{1}H NMR spectrum of compound **8** (400 MHz, CDCl$_3$, rt).
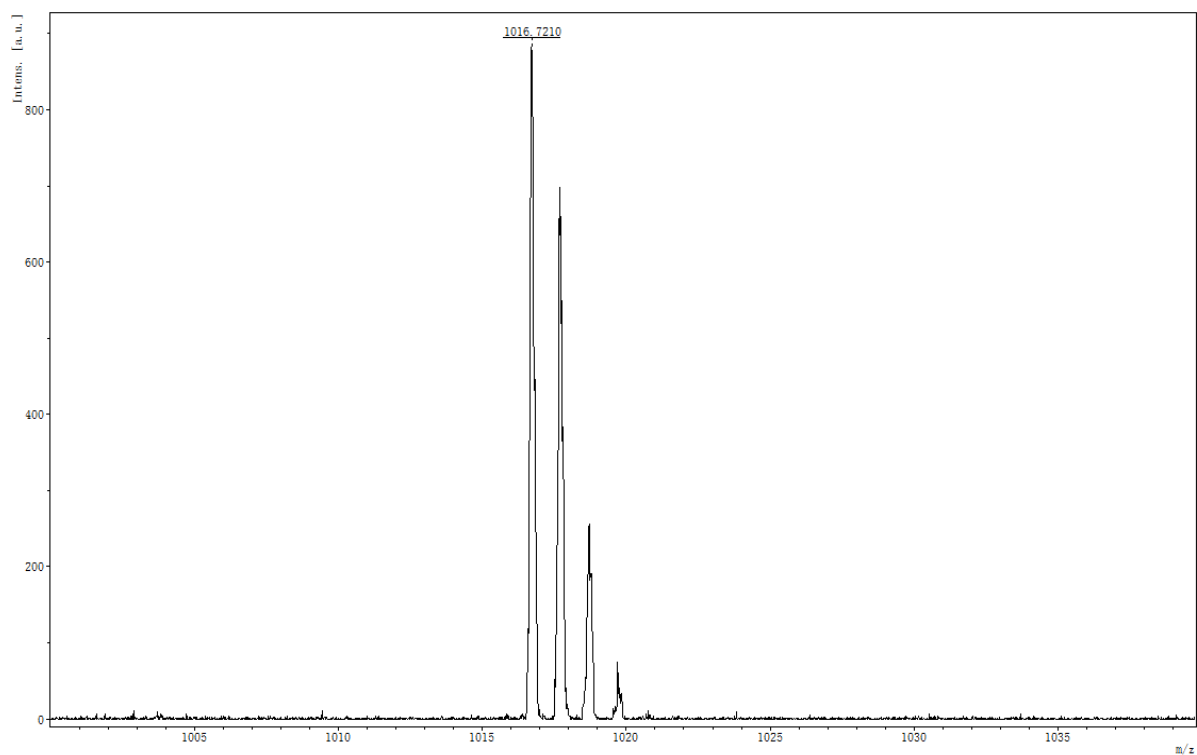
Supplementary Fig. 39. HR (MALDI-TOF) mass spectrum of compound **2**.
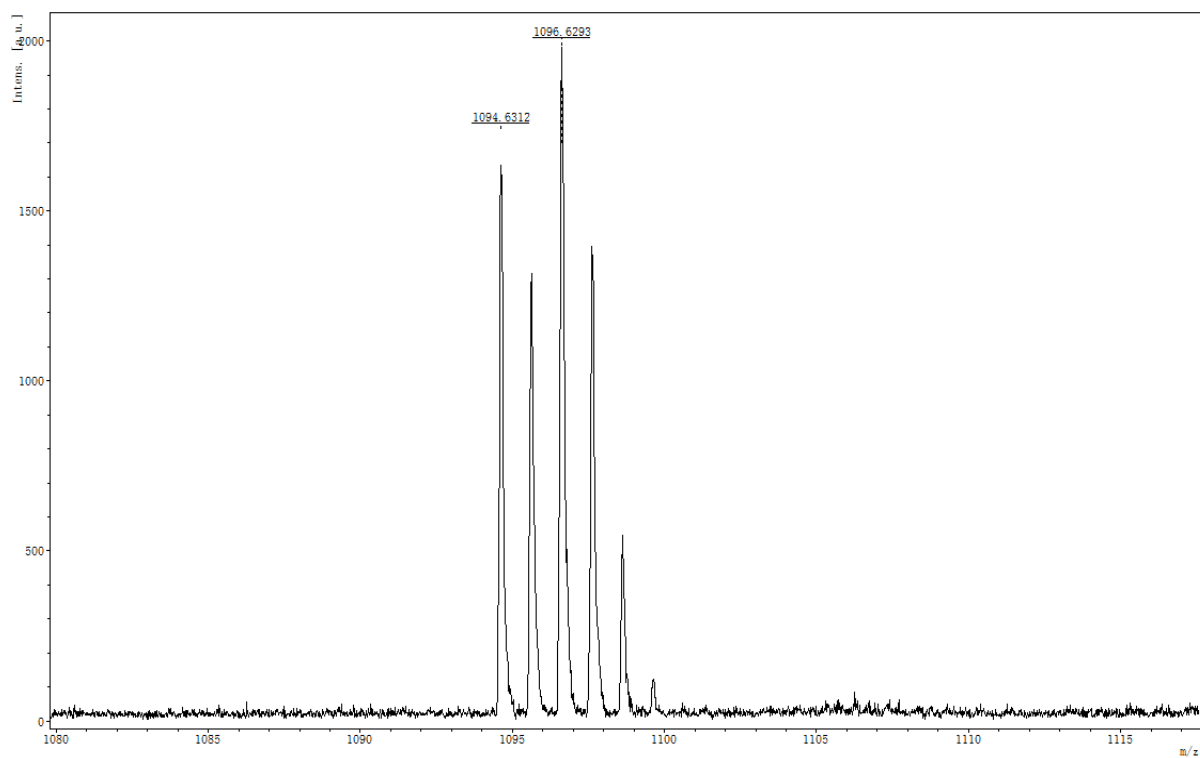
Supplementary Fig. 40. HR (MALDI-TOF) mass spectrum of compound **3**.
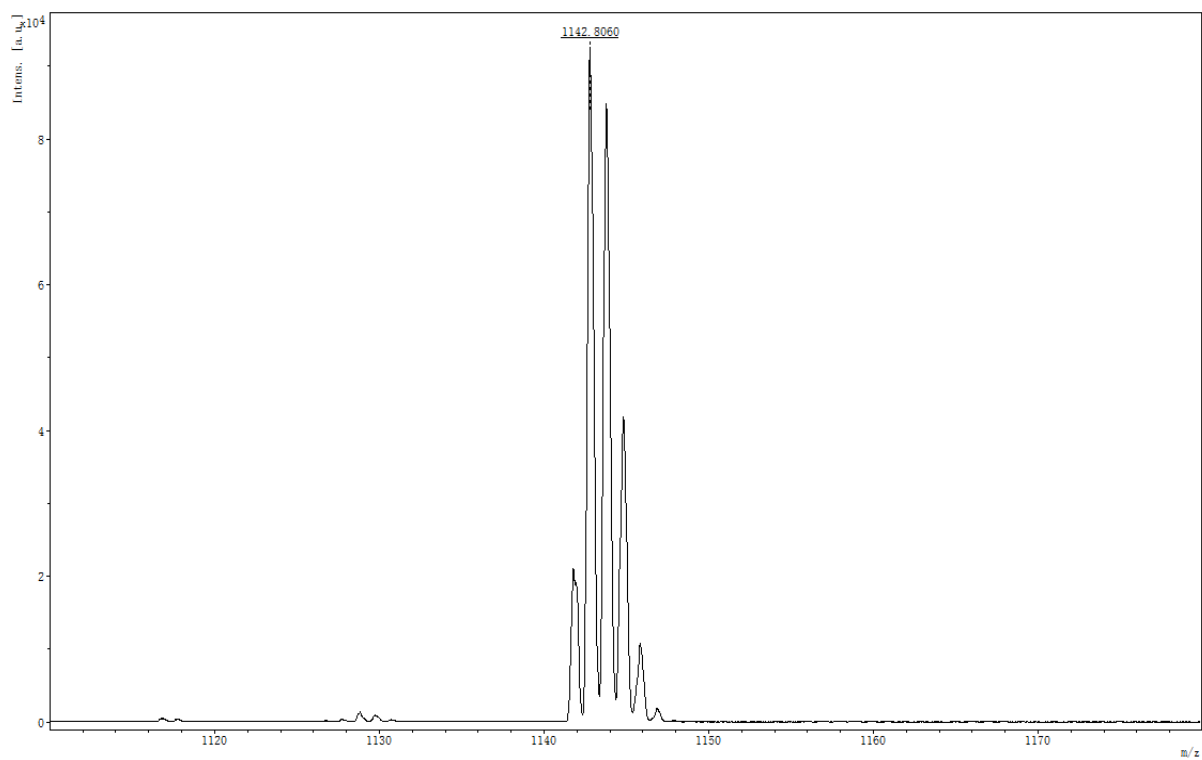
Supplementary Fig. 41. HR (MALDI-TOF) mass spectrum of compound **4**.
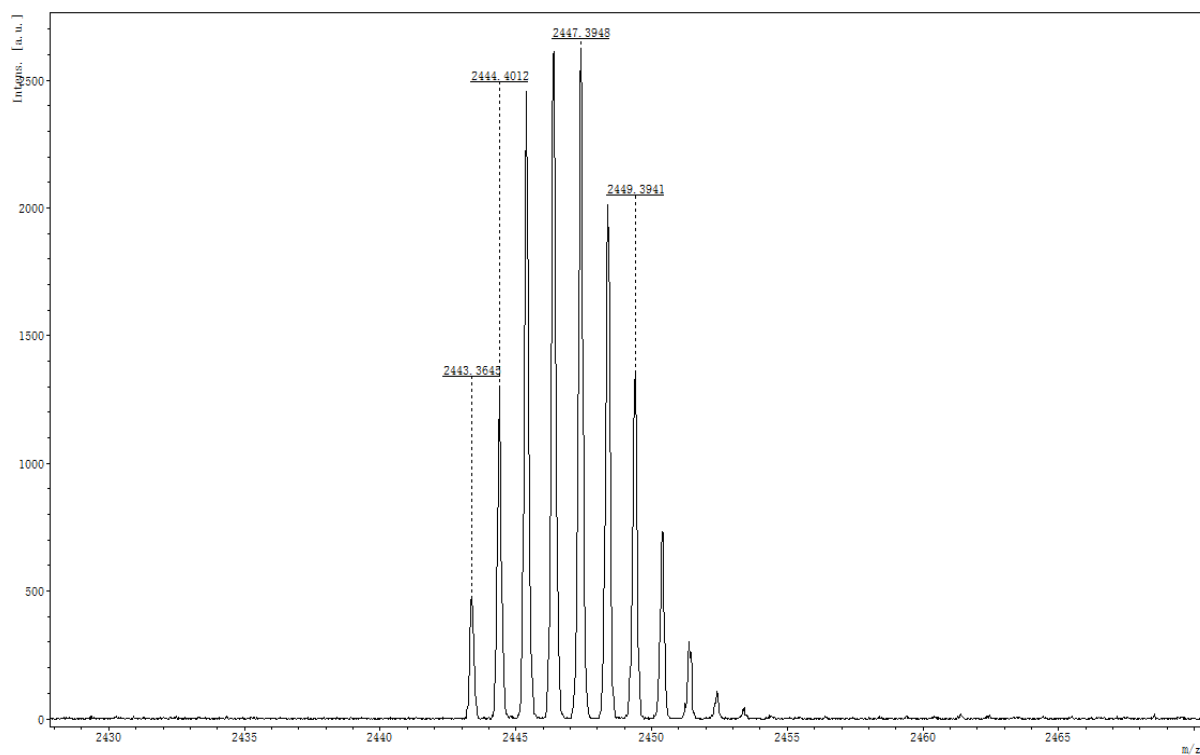
Supplementary Fig. 42. HR (MALDI-TOF) mass spectrum of compound **6**.
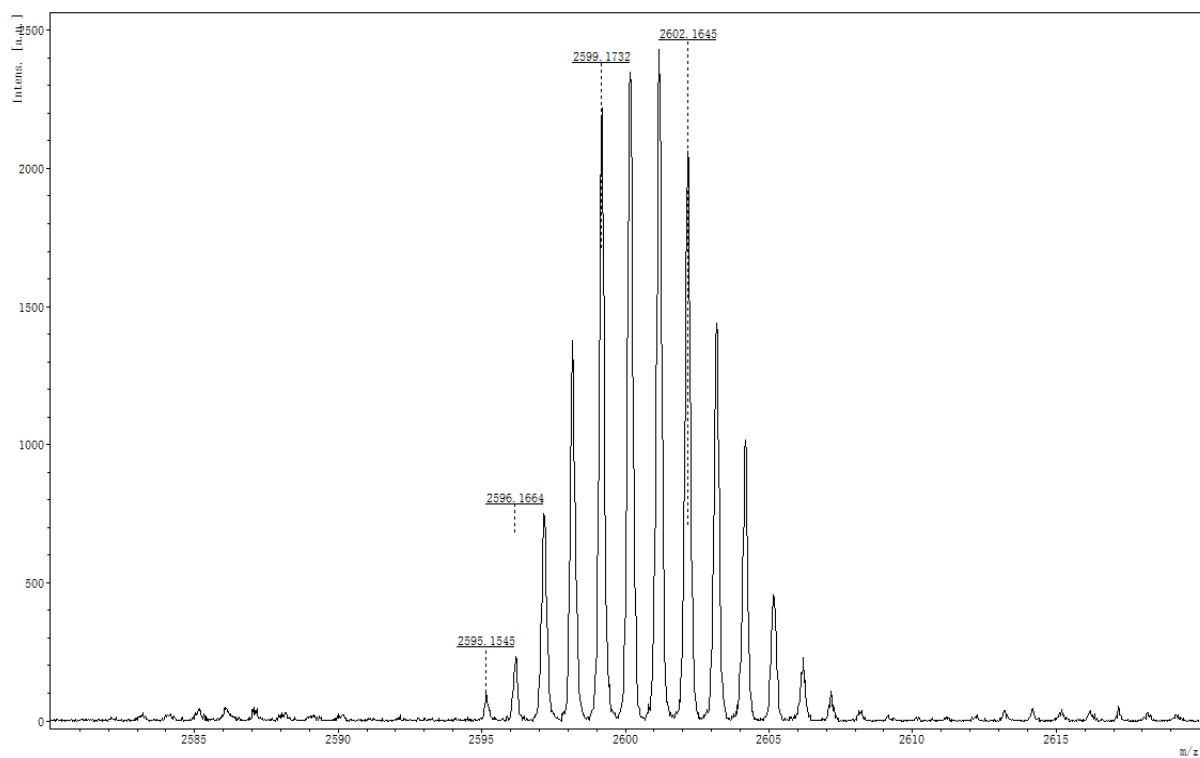
Supplementary Fig. 43. HR (MALDI-TOF) mass spectrum of compound **7**.
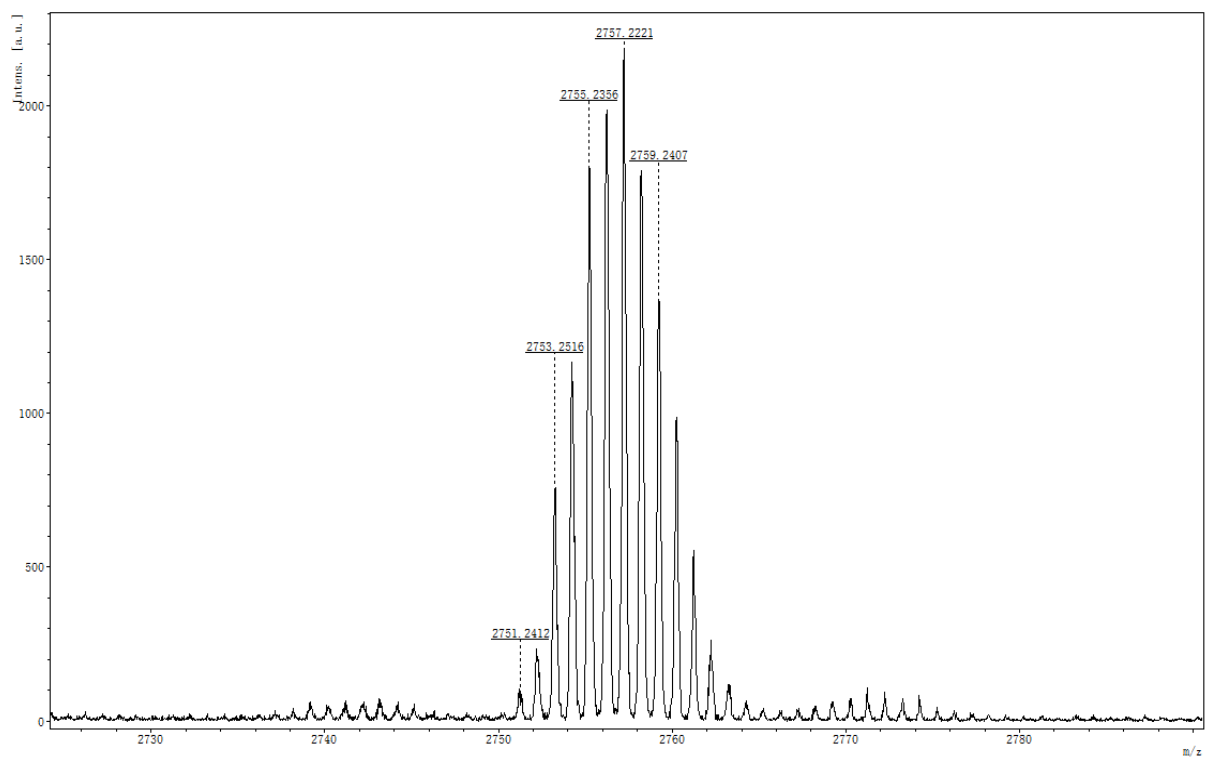
Supplementary Fig. 44. HR (MALDI-TOF) mass spectrum of compound **8**.
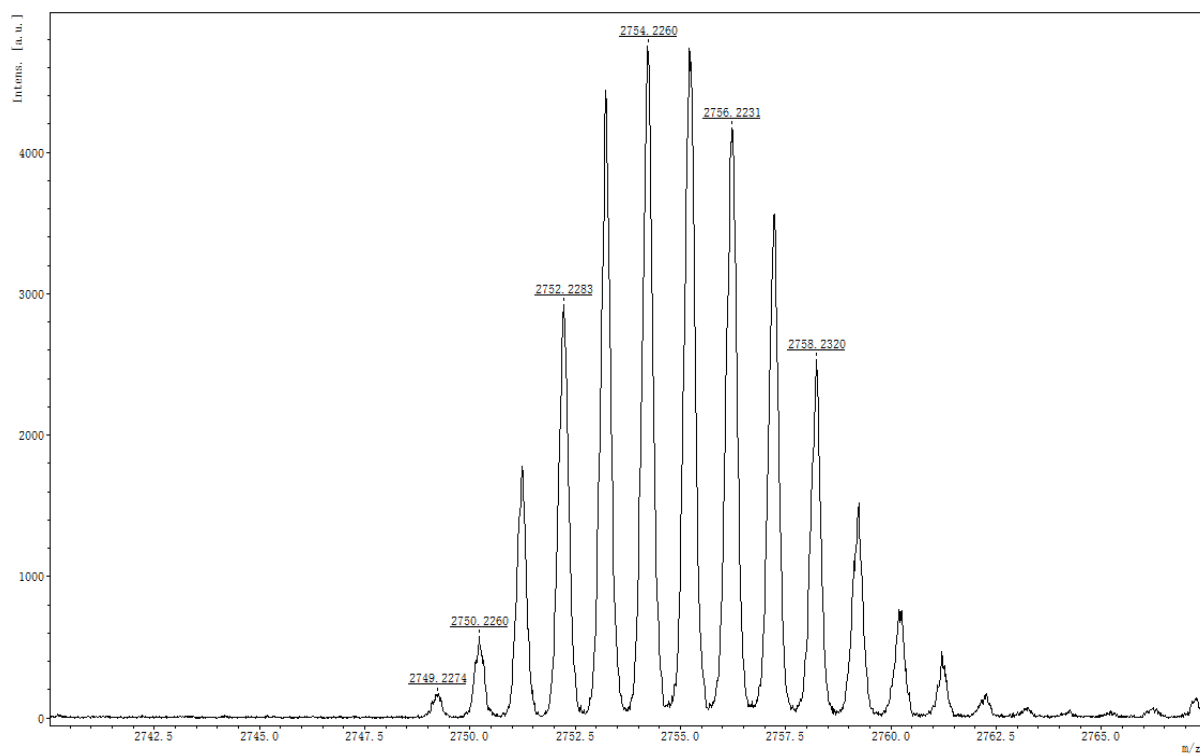
Supplementary Fig. 45. HR (MALDI-TOF) mass spectrum of compound **1**.
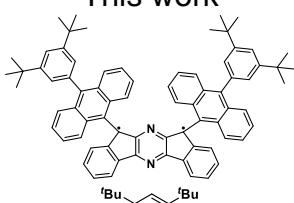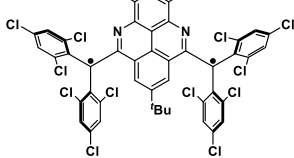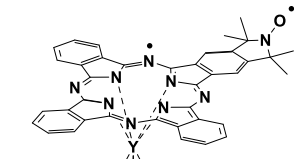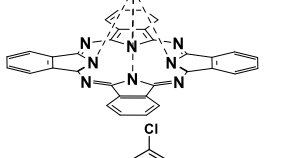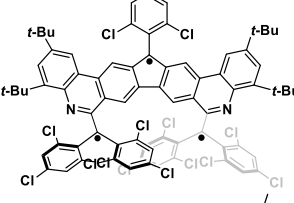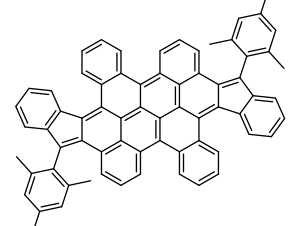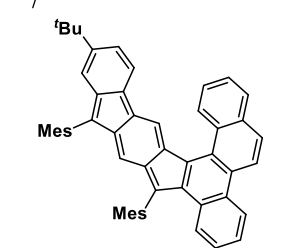
3. Supplementary Tables

Supplementary Table 1. The photophysical and electrochemical data of **1**.

	λ_{max} (nm)	ε_{max} (M^{-1}cm^{-1})	$E_{1/2}{}^{ox}$ (V)	$E_{1/2}{}^{red}$ (V)	HOMO (eV)	LUMO (eV)	$E_g{}^{EC}$ (eV)	$E_g{}^{Opt}$ (eV)
1 (6-PA)	375	177050						
	617	82800						
	645	65600						
	715	19700	0.04	-1.03				
	789	41500	0.32	-1.24	-4.82	-3.76	1.06	0.99
	860	8400						
	1025	3000						
	1090	4950						
	1197	1400						

ε_{max}: molar extinction coefficient at the absorption maximum. $E_{1/2}{}^{ox}$ and $E_{1/2}{}^{red}$ are half-wave potentials of the oxidative and reductive waves, respectively, with potentials *versus* Fc/Fc$^+$ couple. HOMO and LUMO energy levels were calculated according to equations: HOMO = - (4.8 + $E_{ox}{}^{onset}$) eV and LUMO = - (4.8 + $E_{red}{}^{onset}$) eV, where $E_{ox}{}^{onset}$ and $E_{red}{}^{onset}$ are the onset potentials of the first oxidative and reductive redox wave, respectively. $E_g{}^{EC}$: electrochemical energy gap derived from LUMO-HOMO. $E_g{}^{Opt}$: optical energy gap derived from lowest energy absorption onset in the absorption spectra. [a] Y. Li *et.al.*, *J. Am. Chem. Soc.* **2012**, *134*, 14913.

Supplementary Table 2. The molecule structure, spin-lattice relaxation time (T_1) and spin coherence time (T_m) of the radicals[17-21]

Radical structure	T (K)	T_1	T_m	References
This work	70 K	16.7 ms	0.85 μs	-
	100 K	4.3 ms	3.0 μs	*Angew. Chem. Int. Ed.* 2021, 60, 4594-4598.
	50 K	1.47 ms	0.75 μs	*Angew. Chem. Int. Ed.* 2023, 62, e202314900.
	20 K	12.7 ms	14.0 μs	
	90 K	0.4 ms	6.8 μs	*Chem. Eur. J.* 2024, 30, e202400420.
	50 K	1.76 ms	1.78 μs	*J. Am. Chem. Soc.* 2024, 146, 21752-21761.
	T$_1$ up to around 100 ms in solution (both in d-toluene and CS$_2$) at 5 K, T$_m$ up to 290 μs in CS$_2$ at 90 K.			Science, 2019 , 366, 1107-1110.
	T$_1$ up to 1 ms in solid d$_{14}$OTP matrix at room temperature, T$_m$ up to 38 μs in solid d$_{14}$OTP matrix at 200 K.			Chem, 2021, 7, 1363–1378.

Supplementary Table 3. Selected TD-DFT (UB3LYP/6-31G(d,p)) calculated energies, oscillator strength and compositions of major electronic transitions of **1**. H=HOMO, L=LUMO, L+1=LUMO+1, etc.

Wavelength (nm)	Osc. Strength (f)	Major contributions
1080.9	0.1004	H-1(A)→L (A) (37%), H-1(B)→L (B) (33%)
702.1	0.7043	H (A)→L+1(A) (38%), H (B)→L+1(B) (29%)
661.1	0.2603	H-2(A)→L (A) (12%), H-1(A)→L+1(A) (35%), H-2(B)→L (B) (12%), H-1(B)→L+1(B) (31%)
617.9	0.1567	H-2(A)→L (A) (33%), H-1(A)→L+1(A) (12%), H-2(B)→L (B) (34%)
431.3	0.2551	H-4(A)→L (A) (15%), H-1(A)→L+3(A) (10%), H-4(B)→L (B) (19%), H-1(B)→L+3(B) (10%), H-7(A)→L (A) (8%)

Supplementary Table 4. Selected TD-DFT (UB3LYP/6-31G(d,p)) calculated energies, oscillator strength and compositions of major electronic transitions of **1**⋅+. H=HOMO, L=LUMO, LUMO+1=L+1, etc.

Wavelength (nm)	Osc. Strength (ƒ)	Major contributions
1870.05	0.2825	H(B)→L(B) (93%)
1821.69	0.0188	H-1(A)→L(A) (26%), H(B)→L+1(B) (66%)
784.66	0.0149	H-4(A)→L(A) (84%), H-3(A)→L(A) (13%)
705.30	0.044	H-5(A)→L(A) (92%)
684.92	0.0337	H-10(A)→L(A) (12%), H-9(A)→L(A) (17%), H-8(A)→L(A) (50%)
682.09	0.0303	H-12(A)→L(A) (22%), H-10(A)→L(A) (25%), H-9(A)→L(A) (25%)
670.84	0.0167	H-13(A)→L(A) (16%), H-11(A)→L(A) (51%)

Supplementary Table 5. Selected TD-DFT (UB3LYP/6-31G(d,p)) calculated energies, oscillator strength and compositions of major electronic transitions of 1^{2+}. H=HOMO, L=LUMO, LUMO+1=L+1, etc.

Wavelength (nm)	Osc. Strength (f)	Major contributions
1685.71	0.5245	H(A)→L(A) (27%), H(A)→L+1(A) (21%), H(B)→L(B) (40%)
1051.07	0.0246	H-3(A)→L(A) (24%), H-3(A)→L+1(A) (20%), H-3(B)→L(B) (38%)
891.01	0.0082	H-2(A)→L(A) (43%), H-2(A)→L+1(A) (26%), H-1(B)→L(B) (14%)
867.4	0.0076	H-1(A)→L(A) (32%), H-1(A)→L+1(A) (26%), H-3(B)→L+1(B) (21%)
836.21	0.0077	H-1(B)→L(B) (10%), H-1(B)→L+1(B) (71%)

Supplementary Table 6. Selected TD-DFT (RB3LYP/6-31G(d,p)) calculated energies, oscillator strength and compositions of major electronic transitions of **1**. H=HOMO, L=LUMO, LUMO+1=L+1, etc.

Wavelength (nm)	Osc. Strength (f)	Major contributions
652.24	0.4536	H-1→L+1 (94%)
541.65	0.0256	H-4→L (92%)
526.07	0.3332	H-7→L (88%)
490.77	0.0254	H-13→L (20%), H-12→L (62%)

Supplementary Table 7. Selected TD-DFT (RB3LYP/6-31G(d,p)) calculated energies, oscillator strength and compositions of major electronic transitions of 1^{2+}. H=HOMO, L=LUMO, LUMO+1=L+1, etc.

Wavelength (nm)	Osc. Strength (f)	Major contributions
1772.98	0.5477	H→L (103%)
845.96	0.0115	H-1→L+1 (89%)
831.61	0.0117	H-2→L+1 (96%)
788.30	0.0108	H-5→L (88%)
747.20	0.0309	H-4→L+1 (97%)
744.52	0.011	H-5→L+1 (95%)

Supplementary Table 8. Selected TD-DFT (RCAM-B3LYP/6-31G(d,p)) calculated energies, oscillator strength and compositions of major electronic transitions of **1**. H=HOMO, L=LUMO, LUMO+1=L+1, etc.

Wavelength (nm)	Osc. Strength (f)	Major contributions
2822.95	0.212	H→L (105%)
526.07	0.3332	H-7→L (88%)
516.21	0.3772	H-2→L (14%), H-1→L+1 (40%), H→L+2 (42%)
452.76	0.2624	H-5→L (54%)
450.62	0.2038	H-7→L (45%), H-5→L (10%)
433.63	0.2398	H-1→L+1 (37%), H→L+2 (50%)
397.78	0.5941	H-7→L (21%), H-4→L (11%), H→L+5 (31%)
368.23	0.0592	H-23→L (19%), H-22→L (33%), H-21→L (23%)
367.31	0.8121	H-6→L (11%), H-4→L (38%), H-1→L+3 (21%)
366.54	0.1911	H-6→L (56%)

Supplementary Table 9. Selected TD-DFT (RCAM-B3LYP/6-31G(d,p)) calculated energies, oscillator strength and compositions of major electronic transitions of $\mathbf{1^{2+}}$. H=HOMO, L=LUMO, LUMO+1=L+1, etc.

Wavelength (nm)	Osc. Strength (f)	Major contributions
1369.69	0.9396	H→L (97%)
659.49	0.1381	H-1→L+1 (53%), H→L+2 (41%)
491.36	0.1466	H-21→L (10%), H-19→L (10%)
488.78	0.7495	H-3→L (15%), H-1→L+1 (19%), H→L+2 (27%)
482.56	0.5374	H-22→L (10%), H-16→L (12%)
474.09	0.0953	H-22→L (10%), H-10→L (15%)
473.10	0.1166	H-26→L (13%)
463.18	0.1572	H-11→L (16%), H-2→L (13%)
456.53	0.1214	H-3→L (16%)
455.29	0.3781	H-12→L (13%)

Supplementary Table 10. Selected TD-DFT (RωB97XD/6-31G(d,p)) calculated energies, oscillator strength and compositions of major electronic transitions of 1. H=HOMO, L=LUMO, LUMO+1=L+1, etc.

Wavelength (nm)	Osc. Strength (f)	Major contributions
2831.98	0.2797	H→L (101%)
644.17	0.0834	H-2→L (69%), H-1→L+1 (24%)
493.21	0.2778	H-2→L (17%), H-1→L+1 (24%), H→L+2 (51%)
447.06	0.3791	H-19→L (12%), H-7→L (16%), H-5→L (31%), H→L+5 (11%)
396.09	0.3437	H-1→L+1 (46%), H→L+2 (35%)
389.23	1.0686	H-7→L (13%), H→L+5 (47%)
370.69	0.2828	H-1→L+3 (20%), H→L+5 (16%)
354.83	0.1218	H-30→L (31%), H-20→L (17%)
353.12	0.2697	H-22→L (44%), H-21→L (14%)
352.07	0.7128	H-23→L (16%), H-21→L (38%)
351.12	2.3388	H-22→L (26%), H-4→L (13%), H-1→L+3 (24%)

Supplementary Table 11. Selected TD-DFT (RωB97XD/6-31G(d,p)) calculated energies, oscillator strength and compositions of major electronic transitions of $\mathbf{1^{2+}}$. H=HOMO, L=LUMO, LUMO+1=L+1, etc.

Wavelength (nm)	Osc. Strength (ƒ)	Major contributions
1326.89	1.0397	H→L (96%)
639.39	0.1834	H-1→L+1 (44%), H→L+2 (47%)
457.78	1.2033	H-27→L (27%), H-26→L+1 (16%), H-16→L (12%)
452.28	0.9495	H-17→L (12%), H-1→L+1 (32%), H→L+2 (38%)
446.42	0.0339	H-16→L+1 (14%), H-1→L+2 (21%), H→L+3 (15%)
428.83	0.0832	H-20→L (14%)
420.45	0.0145	H-10→L (48%), H-10→L+1 (15%)

Supplementary Table 12. Selected TD-DFT (UCAM-B3LYP/6-31G(d,p)) calculated energies, oscillator strength and compositions of major electronic transitions of **1**$^{\cdot+}$. H=HOMO, L=LUMO, LUMO+1=L+1, etc.

Wavelength (nm)	Osc. Strength (f)	Major contributions
2094.68	0.1643	H-1(B)→L(B) (17%), H(B)→L(B) (75%)
1023.23	0.2482	H-1(A)→L(A) (66%)
852.65	0.347	H-1(A)→L(A) (11%), H(A)→L(A) (64%)
651.49	0.081	H-2(A)→L(A) (25%), H-1(A)→L+1(A) (15%), H(A)→L+1(A) (11%)
528.04	0.07	H-8(B)→L(B) (14%)
488.42	0.3347	H-1(A)→L+1(A) (12%)
451.21	0.1617	H-17(B)→L(B) (10%)
447.79	0.4036	H-5(A)→L(A) (11%), H-1(A)→L+1(A) (20%)
435.51	0.1871	H-27(A)→L(A) (6%), H-25(A)→L(A) (7%), H-23(A)→L(A) (9%), H-

Supplementary Table 13. Selected TD-DFT (UCAM-B3LYP/6-31G(d,p)) calculated energies, oscillator strength and compositions of major electronic transitions of $\mathbf{1^{2+}}$. H=HOMO, L=LUMO, LUMO+1=L+1, etc.

Wavelength (nm)	Osc. Strength (f)	Major contributions
2064.68	0.1807	H(A)→L(A) (36%), H(B)→L(B) (55%)
1312.28	0.0794	H-1(A)→L+1(A) (10%), H-17(A)→L(A) (14%), H-17(B)→L(B) (15%)
520.44	0.2542	H-27(A)→L(A) (7%), H(A)→L+2(A) (8%), H-27(B)→L(B) (7%), H(B)→L+2(B) (8%)
511.32	0.0433	H(A)→L+2(A) (14%), H(B)→L+2(B) (14%)
477.25	0.4232	H(A)→L+2(A) (9%), H(B)→L+2(B) (9%)
474.93	0.0981	H-10(A)→L(A) (12%), H-10(A)→L+1(A) (15%)
471.46	0.6379	H-12(B)→L(B) (8%), H-3(B)→L(B) (6%)

Supplementary Table 14. Selected TD-DFT (UωB97XD/6-31G(d,p)) calculated energies, oscillator strength and compositions of major electronic transitions of **1**. H=HOMO, L=LUMO, LUMO+1=L+1, etc.

Wavelength (nm)	Osc. Strength (f)	Major contributions
655.37	0.0562	H-1(A)→L+1(A) (12%), H(A)→L(A) (21%), H-1(B)→L+1(B) (12%), H(B)→L(B) (23%)
494.95	0.5441	H(A)→L+1(A) (31%), H(B)→L+1(B) (30%)
486.17	0.1406	H-2(A)→L+1(A) (11%), H(A)→L+2(A) (14%), H-2(B)→L+1(B) (11%), H(B)→L+2(B) (14%)
431.93	0.2937	H-1(A)→L(A) (27%), H-1(B)→L(B) (28%)
431.37	1.8738	H-1(A)→L+1(A) (22%), H-1(B)→L+1(B) (23%)
420.57	0.1885	H-2(A)→L(A) (11%), H-1(A)→L+2(A) (10%), H-2(B)→L(B) (12%), H-1(B)→L+2(B) (10%)
380.93	0.0566	H(A)→L+3(A) (7%), H(B)→L+3(B) (8%)

Supplementary Table 15. Selected TD-DFT (UωB97XD/6-31G(d,p)) calculated energies, oscillator strength and compositions of major electronic transitions of **1**$^{·+}$. H=HOMO, L=LUMO, LUMO+1=L+1, etc.

Wavelength (nm)	Osc. Strength (*f*)	Major contributions
2010.12	0.1952	H-1(B)→L(B) (21%), H(B)→L(B) (71%)
970.22	0.2186	H-1(A)→L(A) (68%)
841.77	0.0822	H-1(B)→L(B) (46%), H(B)→L(B) (14%)
777.04	0.3513	H(A)→L(A) (74%)
637.39	0.0999	H-2(A)→L(A) (20%), H-1(A)→L+1(A) (16%), H(A)→L+1(A) (12%)
572.20	0.0704	H-10(B)→L(B) (17%), H-4(B)→L(B) (14%), H(B)→L+1(B) (12%)
527.66	0.0889	H(A)→L+1(A) (16%), H-1(B)→L+1(B) (16%), H(B)→L+1(B) (15%)
504.21	0.1198	H(B)→L+2(B) (12%)
493.31	0.2247	H(A)→L+1(A) (12%), H(B)→L+1(B) (25%)
469.69	0.5032	H(B)→L+1(B) (17%)
447.71	0.1202	H-16(B)→L(B) (10%), H(B)→L+2(B) (14%)
440.71	0.2401	H-16(B)→L(B) (7%), H-1(B)→L+2(B) (5%), H(B)→L+2(B) (5%)
427.59	0.1696	H-22(B)→L(B) (11%)
423.66	0.417	H-1(A)→L+1(A) (12%)

Supplementary Table 16. Selected TD-DFT (UωB97XD/6-31G(d,p)) calculated energies, oscillator strength and compositions of major electronic transitions of $\mathbf{1}^{2+}$. H=HOMO, L=LUMO, LUMO+1=L+1, etc.

Wavelength (nm)	Osc. Strength (f)	Major contributions
1893.18	0.1997	H(A)→L(A) (33%), H(B)→L(B) (56%)
1287.08	0.8726	H-1(A)→L+1(A) (10%), H(A)→L+1(A) (38%), H-1(B)→L+1(B) (10%), H(B)→L+1(B) (31%)
539.60	0.0554	H-17(A)→L(A) (12%), H-17(B)→L(B) (10%)
500.82	0.2252	H-27(A)→L(A) (8%), H-27(B)→L(B) (6%)
485.79	0.0928	H(A)→L+2(A) (10%), H(B)→L+2(B) (11%)
457.88	0.1684	H-12(A)→L(A) (5%), H-12(A)→L+1(A) (5%)
453.09	0.9758	H-27(A)→L+1(A) (5%), H-21(A)→L(A) (4%), H-27(B)→L+1(B) (4%), H-25(B)→L(B) (4%), H-12(B)→L(B) (5%)
452.07	0.3138	H-8(A)→L+1(A) (5%), H(A)→L+2(A) (6%), H(B)→L+2(B) (6%)
451.08	0.2597	H(A)→L+2(A) (6%), H-13(B)→L+1(B) (5%)

Supplementary Table 17.   Crystallographic data for compound **7**.

Identification code	1
Empirical formula	$C_{206}H_{219}Br_2Cl_4N$
Formula weight	3010.43
Temperature	170.0 K
Wavelength	1.34139 Å
Crystal system	Triclinic
Space group	P-1
Unit cell dimensions	a = 19.899(3) Å α = 88.018(5)°.
	b = 20.168(3) Å β = 74.152(5)°.
	c = 24.932(3) Å γ = 71.424(5)°.
Volume	9109(2) Å^3
Z	2
Density (calculated)	1.098 Mg/m^3
Absorption coefficient	0.982 mm^{-1}
F(000)	3200.0
Crystal size	$0.26 \times 0.05 \times 0.03$ mm^3
Radiation	GaKα (λ = 1.34139)
Theta range for data collection	5.294 to 105.962°.
Index ranges	-22<=h<=23, -23<=k<=24, 0<=l<=29
Reflections collected	32135
Independent reflections	32135 [R(sigma) = 0.1490]
Max. and min. transmission	0.752 and 0.513
Refinement method	Full-matrix least-squares on F^2
Data / restraints / parameters	32135/461/1923
Goodness-of-fit on F^2	1.042
Final R indices [I>2sigma(I)]	R1 = 0.1048, wR2 = 0.2784
R indices (all data)	R1 = 0.1643, wR2 = 0.3112
Largest diff. peak and hole	0.80 and -0.99 e.Å^{-3}

Supplementary Table 18.   Crystallographic data for compound **1**.

Identification code	a
Empirical formula	$C_{190}H_{188}Cl_8$
Formula weight	2754.99
Temperature	150.00 K
Wavelength	1.54178 Å
Crystal system	Triclinic
Space group	P-1
Unit cell dimensions	a = 17.5452(6) Å α = 79.219(2)°.
	b = 21.4777(8) Å β = 84.3809(19)°.
	c = 25.5805(8) Å γ = 85.311(2)°.
Volume	9404.0(6) Å^3
Z	2
Density (calculated)	0.973 g/cm^3
Absorption coefficient	1.428 mm^{-1}
F(000)	2928.0
Crystal size	0.23 x 0.18 x 0.16 mm^3
2Θ range for data collection	4.972 to 133.192°
Index ranges	-18<=h<=20, -25<=k<=25, -30<=l<=330
Reflections collected	69560
Independent reflections	33016 [Rint = 0.0593, R$_{sigma}$ = 0.1028]
Date completeness	99.3 %
Max. and min. transmission	0.754 and 0.548
Refinement method	Full-matrix least-squares on F^2
Data / restraints / parameters	33016/3915/2515
Goodness-of-fit on F^2	1.106
Final R indices [I>2sigma(I)]	R$_1$ = 0.1005, wR$_2$ = 0.3061
R indices (all data)	R$_1$ = 0.1493, wR$_2$ = 0.3527
Extinction coefficient	n/a
Largest diff. peak and hole	0.67 and -0.61 e.Å^{-3}

4. Supplementary References

1. Shen, T., et al. Bis-peri-dinaphtho-rylenes: Facile Synthesis via Radical-Mediated Coupling Reactions and their Distinctive Electronic Structures. *Angew. Chem. Int. Ed.* **62**, e202311928 (2023).

2. Ni, Y., et al. A Peri‐tetracene Diradicaloid: Synthesis and Properties. *Angew. Chem. Int. Ed.* **57**, 9697-9701 (2018).

3. Gaussian 16, Revision D.01, Frisch, M. J.; Trucks, G. W.; Schlegel, H. B.; Scuseria, G. E.; Robb, M. A.; Cheeseman, J. R.; Scalmani, G.; Barone, V.; Petersson, G. A.; Nakatsuji, H.; Li, X.; Caricato, M.; Marenich, A. V.; Bloino, J.; Janesko, B. G.; Gomperts, R.; Mennucci, B.; Hratchian, H. P.; Ortiz, J. V.; Izmaylov, A. F.; Sonnenberg, J. L.; Williams-Young, D.; Ding, F.; Lipparini, F.; Egidi, F.; Goings, J.; Peng, B.; Petrone, A.; Henderson, T.; Ranasinghe, D.; Zakrzewski, V. G.; Gao, J.; Rega, N.; Zheng, G.; Liang, W.; Hada, M.; Ehara, M.; Toyota, K.; Fukuda, R.; Hasegawa, J.; Ishida, M.; Nakajima, T.; Honda, Y.; Kitao, O.; Nakai, H.; Vreven, T.; Throssell, K.; Montgomery, J. A., Jr.; Peralta, J. E.; Ogliaro, F.; Bearpark, M. J.; Heyd, J. J.; Brothers, E. N.; Kudin, K. N.; Staroverov, V. N.; Keith, T. A.; Kobayashi, R.; Normand, J.; Raghavachari, K.; Rendell, A. P.; Burant, J. C.; Iyengar, S. S.; Tomasi, J.; Cossi, M.; Millam, J. M.; Klene, M.; Adamo, C.; Cammi, R.; Ochterski, J. W.; Martin, R. L.; Morokuma, K.; Farkas, O.; Foresman, J. B.; Fox, D. J. Gaussian, Inc., Wallingford CT, 2016.

4. Becke, A. D. Density-functional thermochemistry. III. The role of exact exchange. *J. Chem. Phys.* **98**, 5648-5652 (1993).

5. Lee, C., Yang, W., Parr, R. G. Development of the Colle-Salvetti correlation-energy formula into a functional of the electron density. *Phys Rev B.* **37**, 785-789 (1988).

6. Yanai, T., Tew, D. P., Handy, N. C. A new hybrid exchange–correlation functional using the Coulomb-attenuating method (CAM-B3LYP). *Chem Phys Lett.* **393**, 51-57 (2004).

7. Ditchfield, R., Hehre, W. J., Pople, J. A. Self-Consistent Molecular-Orbital Methods. IX. An Extended Gaussian-Type Basis for Molecular-Orbital Studies of Organic Molecules. *J. Chem. Phys.* **54**, 724-728 (1971).

8. Hehre, W. J., Ditchfield, R., Pople, J. A. Self—Consistent Molecular Orbital Methods. XII. Further Extensions of Gaussian—Type Basis Sets for Use in Molecular Orbital Studies of Organic Molecules. *J. Chem. Phys.* **56**, 2257-2261 (1972).

9. Hariharan, P. C., Pople, J. A. J. T. c. a. The influence of polarization functions on molecular orbital hydrogenation energies. *Theoret.chim.Acta.* **28**, 213-222 (1973).

10. Yamanaka, S., Okumura, M., Nakano, M., Yamaguchi, K. J. J. o. M. S. EHF theory of chemical reactions part 4. UNO CASSCF, UNO CASPT2 and R (U) HF coupled-cluster (CC) wavefunctions. *J. Mol. Struct.* **310**, 205-218 (1994).

11. Kamada, K., et al. Singlet Diradical Character from Experiment. *J. Phys. Chem. Lett.* **1**, 937-940 (2010).

12. Geuenich, D., Hess, K., Köhler, F., Herges, R. J. C. r. Anisotropy of the induced current density (ACID), a general method to quantify and visualize electronic delocalization. *Chem. Rev.* **105**, 3758-3772 (2005).

13. Chen, Z., Wannere, C. S., Corminboeuf, C., Puchta, R., Schleyer, P. v. R. J. C. r. Nucleus-independent chemical shifts (NICS) as an aromaticity criterion. *Chem. Rev.* **105**, 3842-3888 (2005).

14. Fallah-Bagher-Shaidaei, H., Wannere, C. S., Corminboeuf, C., Puchta, R., Schleyer, P. v. R. J. O. L. Which NICS aromaticity index for planar π rings is best? *Org. Lett.* **8**, 863-866 (2006).

15. Sabrina Klod and Erich Kleinpeter. Ab initio calculation of the anisotropy effect of multiple bonds and the ring current effect of arenes—application in conformational and configurational analysis. *J.Am.Chem.Soc*. **2**, 1893-1898 (2001).

16. Lu, T., Chen, F. Multiwfn: A multifunctional wavefunction analyzer. J. Comput. Chem. **33**, 580-592 (2011).

17. Lombardi, F., Lodi, A., Ma, J., Liu, J., Slota, M., Narita, A., Myers,W. K., Mullen, K., Feng, X. L., Bogani, L. Quantum Units From the Topological Engineering of Molecular Graphenoids. *Science*, **366**, 1107-1110 (2019).

18. Lombardi, F., Ma, J., Alexandropoulos, D. I., Komber, H., Liu, J.Myers, W. K., Feng, X. Bogani, L. Synthetic Tuning of the Quantum Properties of Open-shell Radicaloids. *Chem* **7**, 1363–1378 (2021).

19. Wolfowicz, G., et al. Author Correction: Quantum guidelines for solid-state spin defects. *Nat. Rev. Mater.* **6**, 1191-1191 (2021).

20. Graham, M. J., Yu, C. J., Krzyaniak, M. D., Wasielewski, M. R., Freedman, D. E. Synthetic Approach to Determine the Effect of Nuclear Spin Distance on Electronic Spin Decoherence. *J. Am. Chem. Soc.* **139**, 3196-3201 (2017).

21. Winpenny, R. E. P. Quantum Information Processing Using Molecular Nanomagnets As Qubits. *Angew. Chem. Int. Ed.* **47**, 7992-7994 (2008).